FACULDADE DE CIÊNCIAS DA SAÚDE

Centro de Investigação em Ciências da Saúde
Health Sciences Research Centre

ELECTRON TRANSFER BIOCHEMISTRY

METAL REDUCTASE ACTIVITY OF TRIHEME CYTOCHROME C_3

EDUARDO PAULO DE OLIVEIRA LOPES CALÇADA

DISSERTATION PRESENTED TO OBTAIN A MSC DEGREE IN BIOCHEMISTRY AT THE FACULDADE DE CIÊNCIAS DA SAÚDE, UNIVERSIDADE DA BEIRA INTERIOR

SUPERVISORS: RICARDO O. LOURO & ILÍDIO J. CORREIA
OPPONENT: LUÍS PASSARINHA

COVILHÃ | 2009

Acknowledgements

A investigação subjacente a esta tese foi o resultado culminar do esforço comum onde orientadores, professores, amigos e restante comunidade científica fora desta instituição desenvolveram um papel importante. Sem eles, nunca teria acesso ao vasto conhecimento inerente e esta investigação nunca teria sido possível.

Ao meu orientador Prof. Doutor Ricardo Louro a audácia, a lucidez e a confiança concedida no presente trabalho, assim como o apoio incondicional na resolução dos problemas que surgiram no desenvolvimento do mesmo;

Ao Prof. Doutor Ilídio Correia pela ousadia de me encaminhar rumo a novos desafios;

Ao Prof. Doutor Carlos Romão pelo apoio e aconselhamento no uso e síntese dos ferrocenos no seu laboratório.

Ao Doutor Yann Astier pela ajuda na familiarização com o potenciostato, assim como nas dúvidas relacionadas com electroquímica.

À Doutora Catarina Paquete pelo empenho, cooperação e perseverança reveladas, assim como nos aconselhamentos e apoio na interpretação tanto das bases cinéticas, como dos procedimentos laboratoriais.

À Engenheira Isabel Pacheco pela simpatia e disponibilidade;

Aos colegas de laboratório Alexandra, Bruno e Ivo, que permitiram toda a harmonia e boa disposição no ambiente laboratorial;

Ao Doutor Lukas Kromer pela ajuda na síntese organometálica dos ferrocenos no laboratório do Doutor Carlos Romão.

Aos amigos que sempre acompanharam o ultrapassar de cada etapa, Ana, Carlos, Diana, Leitão, Márcia, Nelson, Ricardo, Rodrigo, Rute e Teresa.

À minha namorada Adelaide Santos pela ubiquidade em todas as emoções, e por ter sido sempre o alicerce essencial de subtileza e determinação.

À família que se divide por Viseu e pela Guarda. Aos meus pais, a quem com saudade dedico esta tese.

Abbreviations

D. acetoxidans	*Desulfuromonas acetoxidans*
DIRB	Dissimilatory iron-reducing bacteria
DSMZ	Deutsche Sammlung von Mikroorganismen und Zellkulturen GmbH (German Collection of Microorganisms and Cell Cultures)
DEAE	Diethylaminoethyl
DFF	DEAE Fast-Flow column
SDS	Sodium dodecyl sulfate
PAGE	Polyacrylamide gel electrophoresis
OD	Optical density
IUPAC	International union of pure and applied chemistry
NMR	Nuclear magnetic resonance
SRB	Sulfate reducing bacteria
Fc	Ferrocene
SCE	Saturated Calomel Electrode
SHE	Standard Hydrogen Electrode

Keywords

Electron transfer; Kinetics; Cytochrome *c*; Metal reductase; Bioremediation; Organometallics;

Resumo

Os microrganismos anaeróbicos isolados de sedimentos, como *Desulfuromonas acetoxidans* apresentam um mecanismo respiratório de notável versatilidade. Este microrganismo Gram-negativo é estritamente anaeróbio, capaz de adaptar o seu metabolismo a uma vasta gama de aceitadores de electrões, como elementos tóxicos e metais insolúveis. Da grande variedade de citocromos que este microrganismo apresenta, o citocromo c_7 é o mais abundante, e está evolvido na redução de metais. Esta pequena proteína (9kDa) contém três hemos tipo-*c* com coordenação axial bis-histidina. A sua estrutura tridimensional e o arranjo dos três hemos é análoga ao dos citocromos c_3 tetrahémicos de bactérias redutoras de sulfato. No entanto, apresenta diferentes propriedades termodinâmicas e cinéticas. Compreender os mecanismos moleculares da transferência electrónica na cadeia respiratória tem-se tornado um grande desafio. Foi demonstrado que o ambiente electrostático do citocromo c_7, é o parâmetro mais influente que condiciona o local de ligação para a reacção de transferência de electrões entre parceiros redox. O conhecimento detalhado do comportamento desta proteína na transferência de electrões na cadeia respiratória contribuirá para optimizar potencias aplicações de *Desulfuromonas acetoxidans* na biorremediação de ambientes contaminados com metais pesados e também na construção de células de combustível microbianas.

Abstract

Anaerobic microorganisms isolated from sediments such as *Desulfuromonas acetoxidans* displays a remarkably versatile respiratory mechanism. These microorganisms are Gram-negative, strictly anaerobic bacteria, capable of adapting their metabolism to a wide range of electron acceptors, like toxic elements and insoluble metals. From the large variety of cytochromes from these microorganisms, cytochrome c_7 is the most abundant, being a small (9kDa) protein that contains three *c*-type hemes with bis-hystidinyl axial coordination. This protein participates in the reduction of metals. It presents a similar three-dimensional fold as well a conserved arrangement of the three hemes analogous to the tetraheme cytochrome c_3 from sulfate reducing bacteria. However it presents different thermodynamic and kinetic properties. Understanding the molecular mechanisms of the electron transfer in the respiratory chain became a major challenge. It was demonstrated that electrostatic environment of cytochrome c_7 is the major factor that controls the binding site of redox partners in electron transfer reactions.

Detailed knowledge of the behaviour of this protein in the respiratory electron transfer chain will provide the basis for optimization of applications of *Desulfuromonas acetoxidans* in bioremediation and also in the development of microbial fuel cell technology.

Table of Contents

ACKNOWLEDGEMENTS I

ABREVIATIONS ERROR! BOOKMARK NOT DEFINED.

KEYWORDS III

LIST OF FIGURES IX

LIST OF TABLES XI

LIST OF EQUATIONS XI

PREFACE XII

1 INTRODUCTION 1

1.1 Biogeochemisty 1
1.1.1 Metal-reducing bacteria 1
1.1.2 Respiratory Proteins 5

1.2 Electron transfer 8
1.2.1 Marcus Theory 8
1.2.2 Thermodynamic and Kinetic modelling 9

1.3 Biorganometallics 14
1.3.1 Ferrocenes 15
1.3.2 Cobalt complexes 16

2 MATERIALS AND METHODS 18

2.1 Source of organisms 18

2.2 Cell cultivation 18
2.2.1 Growth of Stock cultures 18

2.2.2 Cellular growth using Fumarate as the terminal electron acceptor 19
2.2.3 Cellular growth using Sulphur as the terminal electron acceptor 20
2.2.4 Large scale cell cultivation 20

2.3 Protein Purification 21
2.3.1 Cell harvest and disruption 21
2.3.2 Separation of soluble from membrane fractions 22
2.3.3 Protein purification 22
2.3.4 UV-Visible spectroscopy 23
2.3.5 NMR spectroscopy 25
2.3.5.1 Sample preparation 25
2.3.5.2 NMR spectroscopy 26

2.4 Ferrocenium sample preparation 26
2.4.1 Ferrocene synthesis: 2-Ferrocenylethanol 27
2.4.2 NMR Spectroscopy of ferrocenes 28
2.4.3 Ferrocene oxidation 28
2.4.4 Voltammetry studies 29
2.4.5 UV-Visible spectroscopy 30

2.5 Sample preparation of Cobalt complexes 30
2.5.1 Trans-diclrobis(ethylenediamine)coalt(III) 30
2.5.2 Cis-diclrobis(ethylenediamine)coalt(III) 31
2.5.3 Voltammetry studies 31
2.5.4 UV-Visible spectroscopy 31

2.6 Kinetic Studies 32
2.6.1 Circuit washing 32
2.6.2 Circuit refill procedure 33
2.6.3 Dead time calculation 33
2.6.4 Experimental assay 35
2.6.4.1 Light calibration and circuit refill 35
2.6.4.2 Preparation of mono-substituted ferrocenes 36
2.6.4.3 Sodium dithionite sample preparation 36
2.6.4.4 Preparation of cytochromes samples 36
2.6.5 Kinetic Modelling 37

3 RESULTS 38

3.1 Bacterial growth 38

3.2 Protein Purification 38

3.3 NMR spectroscopy of protein 42

3.4 Ferrocene as mediator 43

3.4.1 Ferrocenylethanol synthesis 43
3.4.2 NMR spectroscopy of ferrocenes 43
3.4.3 Voltammetry of mono-substituted ferrocenes 45
3.4.1 Ferrocene oxidation 46
3.4.2 UV-Visible Spectroscopy of ferrocenes 47

3.5 Cobalt complexes as mediator 49
3.5.1 Synthesis of [*trans*-$Co(en)_2Cl_2]^+$ and [*cis*-$Co(en)_2Cl_2]^+$ 49
3.5.2 Voltammetry 49
3.5.3 UV-Visible Spectroscopy 51

3.6 Stopped-flow calibration dead time 53

3.7 Kinetic experiments 55
3.7.1 Kinetic data using α-Hydroxyethyl ferrocenium as mediator 55
3.7.2 Kinetic data using *Trans*-$[Co(en)_2Cl_2]^+$ as mediator 57

4 DISCUSSION 59

4.1 Mono-substitued ferrocenium as mediator 59

4.2 Cobalt complexes as mediators 60

5 CONCLUSION 67

6 BIBLIOGRAPHY 70

List of Figures

Figure 1.1 – The microbial mediated iron redox cycle 3
Figure 1.2 – Phylogenety affiliation of microorganisms contributing to iron redox cicling 4
Figure 1.3 – Structure and distance metrics of fully reduced *D. acetoxidans* cytochrome c_7 6
Figure 1.4 – Schematic representation of the microstates of a protein with three redox centres and one acid-base centre 10
Figure 1.5 - *Cis-trans* isomeriaztion Dichlorobis(ethylenediamine)cobalt 17
Figure 2.1 – French-Press equipment in use with fast-flow anaerobic kit 22
Figure 2.2 – Stopped-flow equipment 32
Figure 2.3 – Cartoon of dead time determination 35
Figure 3.1 – Scale-up procedure for large-scale growth of *D. acetoxidans* 38
Figure 3.2 - Schematic representation of protein purification 39
Figure 3.3 – SDS-PAGE haem staining 39
Figure 3.4 –UV-Visible DEAE fractions Spectra 40
Figure 3.5 – SDS-PAGE haem staining 41
Figure 3.6 –UV-Visible fraction B spectra from HTP column separation 41
Figure 3.7 – ^{1}H-NMR spectrum of purified cytochrome c_7 42
Figure 3.8 - Ferrocenylethanol synthesis 43
Figure 3.9 - NMR spectra of ferrocenylacetic acid 44
Figure 3.10 - NMR spectra of ferrocenylethanol synthesized in this work. 44
Figure 3.11 - Voltammetry of mono-substituted ferrocenes 45
Figure 3.12 – α-hydroxyethyl ferrocene electrochemical oxidation 46
Figure 3.13 –UV-Visible spectroscopy of mono-substituted ferrocenes 48
Figure 3.14 – Synthesis dichlorobis(ethylenediamine)cobalt(III) 49
Figure 3.15 - Voltammetry of cobalt complexes 50
Figure 3.16 – UV-Visible spectroscopy of *trans*-dichlorobis(ethylenediamine) cobalt(III) in different solvents 51

Figure 3.17 – UV-Visible spectroscopy of *trans* and *cis*-dichlorobis (ethylenediamine) cobalt(III) in different pH buffer solutions 52
Figure 3.18 - Dead time kinetic traces of DCPIP reaction with ascorbic acid 54
Figure 3.19 - Trend line of dead time determination 54
Figure 3.20 – Kinetic traces of the oxidation of *D. gigas* cytochrome c_3 by α-hydroxyethyl ferrocenium 56
Figure 3.21 – UV-visible spectroscopy of cytochrome c_3 57
Figure 3.22 - Kinetics of oxidation of cytochrome c_7 by *trans*-$[Co(en)_2Cl_2]^+$ 58
Figure 4.1 – Electrostatic environment around the hemes of fully reduced cytochrome c_7 from *D. acetoxidans* 64

List of Tables

Table 2.1 – Ascorbic acid *versus* DCPIP solution preparation 34
Table 3.1 – Absorbance values from each fraction from DEAE column. 40
Table 3.2 – Reduction potentials of mono-substituted ferrocenes 47
Table 3.3 – Reduction potential of cobalt complexes 51
Table 3.4 – Reference rate constants for each heme of *D. acetoxidans* cytochrome c_7 58
Table 4.1 – Thermodynamic parameters of cytochrome c_7 from *D. acetoxidans* 62
Table 4.2 – Fraction of electrons that enter and leave the cytochrome c_7 through each heme in each one-electron reduction step. 66

List of Equations

Equation 1.1 - Marcus equation 8
Equation 1.2 - Kinetic model based on Marcus equation 13
Equation 2.1 - Beer-Lambert law 24

Preface

In the present thesis the metal reductase activity of cytochrome c_7 was studied. The presentation of this work is divided in five sections.

The introduction begins with a briefly synopsis about anaerobic microorganisms with the ability to reduce metals and ends with a description of the organometallic compounds used as mediators in this study. These two issues are linked by the description of the Marcus electron transfer theory as well the kinetic model used. The cytochrome c_7 was the focus protein in this study. The cytochrome c_3 was also used but only for the optimization of the kinetic procedure. Two groups of metal complexes were used as mediators: mono-substituted ferrocenes and cobalt complexes.

The materials and methods presents in detail all the procedures used. The main experimental procedures used in this work, such as Stopped-flow and NMR techniques are described in this section.

The presentation of the results includes the analyses and observations registered in every step both for the obtaining of the protein and for the attainment of the redox partner. The modelling of the data and kinetic analysis is discussed both for mono-substituted ferrocenes as well for cobalt complexes.

The conclusion remarks consider the understanding of results and include new targets to be applied in the future.

1 Introduction

1.1 Biogeochemistry

The primary inhabitants of sediments are prokaryotes whose diversity is expressed in terms of metabolism rather than structure because they have optimized their biochemistry for the uptake and utilization of a wide variety of nutrients, like acetate, ethanol or propanol (Gebhardt *et al.* 1985, Nealson & Saffarini 1994). The characteristic vertical nutrient (electron donor and electron acceptor) profiles seen in sediments are produced as a result of microbial activities, with each nutrient a product or reactant of one or more metabolic groups (Nealson 1997).

1.1.1 Metal-reducing bacteria

Iron respiration has been proposed as one of the first forms of microbial metabolism to have evolved, preceding the development of oxygen, nitrate and sulfate respiration (Vargas *et al.* 1998).

For many years, the profiles of metals were regarded as the result of chemical reactions in sediment, primarily because the substrates involved were solids (Mn and Fe oxides) and thought to be inaccessible to direct bacterial reduction. This view has changed dramatically with the discovery of several groups of bacteria that grow by the dissimilatory reduction of

iron and/or manganese (Lovley & Phillips 1988, Lovley 1993, Nealson & Saffarini 1994) which results in the oxidation of organic matter and the reduction of Fe(III) or Mn(IV). A wide variety of iron oxide and iron-bearing clay minerals (representing >90% of oxidative capacity in many environments) can serve as source of Fe(III) for use by dissimilatory iron-reducing bacteria (DIRB). These bacteria performs the reduction of ferric iron Fe(III) to ferrous Fe(II) in anoxic non-sulfidogenic environments, being the fundamental catalysts in iron biogeochemistry (Fredrickson & Gorby 1996).

At pH 7 iron (Fe) exists primarily as insoluble, solid-phase minerals in the divalent ferrous, Fe(II), or trivalent ferric, Fe(III), oxidation states (Cornell & Schwertmann 2003).

Coupled to Fe(III) reduction, microbial catabolism of organic contaminants can occur naturally (Lovley et al. 1989). Fe(III) represents the single most abundant electron acceptor for oxidation of contaminants in many subsurface environments (Fredrickson & Gorby 1996) for lithotrophic and heterotrophic Fe(III)-reducing microorganisms (Weber *et al.* 2006) (figure 1.1).

The activity of DIRB results in the generation of aqueous Fe(II) (aq), and solid-phase Fe(II)-bearing minerals Fe(II)(s) including siderite, vivianite and geologically significant mixed-valence Fe(II)–Fe(III) minerals, such as magnetite and green rust (Lovley 1991).

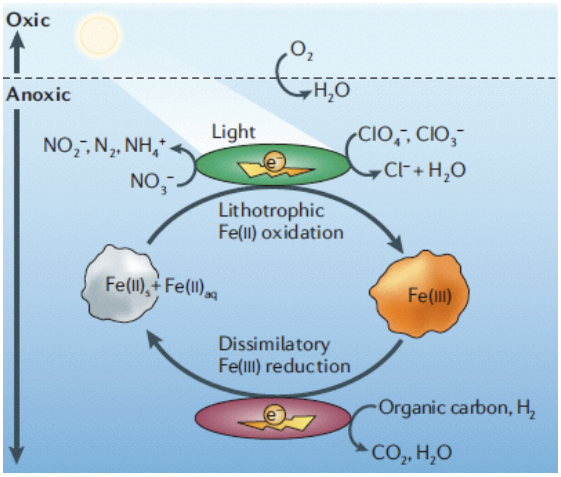

Figure 1.1 – The microbial mediated iron redox cycle (Weber *et al.* 2006).

The physiology of microbial Fe(III) reduction and Fe(II) oxidation remains an enigma, as a terminal Fe(III) reductase has not yet been identified and nothing apart from the implicated role of *c*-type cytochrome(s) is known on Fe(II) oxidation at circumneutral pH (Weber *et al.* 2006).

Desulfuromonas (*D.*) *acetoxidans* has been shown to use Fe(III) as a terminal electron acceptor for growth (Roden & Lovley 1993). *D. acetoxidans* is a strictly anaerobic, rod-shaped, laterally flagellated, Gram-negative bacterium first isolated from marine sediments in 50m depth in the Antarctic ocean at the South Orkney Islands (Pfennig & Biebl 1976). *D. acetoxidans* is involved in a symbiotic association with a green sulfur bacterium in the habitats from which it is isolated (Pfennig & Biebl 1976). The phylogeny of these bacteria (figure 1.2) belongs to the δ-proteobacteria of microorganisms involved in redox cycle of iron (Weber *et al.* 2006).

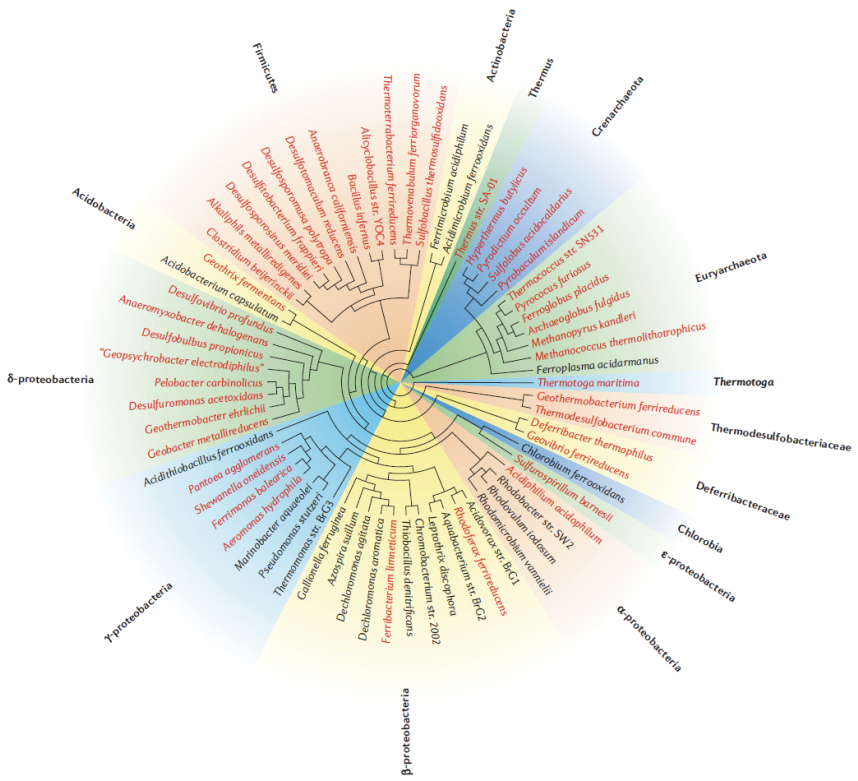

Figure 1.2 – Phylogeny affiliation of microorganisms contributing to iron redox cycling (Weber *et al.* 2006) based on nearly complete 16S ribosomal DNA sequences.

Because it is difficult to grow in laboratory, *D. acetoxidans* is one of the least studied metal-reducing microorganisms. Previous work revealed new methodologies for large scale cell cultivation in the laboratory (Fonseca 2007).

The draft genome of *Desulfuromonas acetoxidans* DSM684 is available on the United States Department of Energy (DOE) Joint Genome Institute (JGI). Knowing the whole genome from *D. acetoxidans* is an advantage for the assembly and correlation of unknown proteins from putative purification and sequence.

1.1.2 Respiratory Proteins

D. acetoxidans contains a multitude of redox proteins that are involved in its respiratory capabilities (Rache et al. 1983).

Hemeproteins such as cytochromes are widespread in living organisms being components of different biological processes. It has been proposed that one-electron transfer occurs to stimulate reduction of metal oxides performed by cytochromes (Brown et al. 1999). The purification of cytochromes with ability to reduce metal oxides offers the possibility of study cell-free metal dissolution. *C*-type hemes are covalently bound to the polypeptide chain, through thioether linkages between the porphyrin vinyl side-chains and cysteinyl residues (Moore & Pettigrew 1990). In all hemeproteins the iron is five or six-coordinated, and these axial ligands are provided by aminoacids of the polypeptide chain as well by other compounds like NO, O_2 or CO. Five-coordinated hemes are high-spin in both oxidation states. Six coordinated hemes (the sixth ligand is usually either a methionine or a histidine) are usually low-spin in both oxidation states. The hemeproteins cover a wide range of reduction potentials (from -500 mV to +400 mV) (Moore & Pettigrew 1990), allowing these proteins to be found in the electron transfer chains of anaerobic and aerobic organisms. The reduction potential of the hemes depends on multiple inter-playing factors, such as electric charges, distance between amino acid residues, dipolar and hydrogen-bonding interactions, solvent exposure, and heme-

heme interactions (homotropic interactions) (Moore & Pettigrew 1990).

The cytochrome c_7 formerly known as cytochrome $c_{551,5}$ is the most abundant cytochrome in the periplasm of *D. acetoxidans* (Giudici-Orticoni et al. 2003). It is a 68 amino acid monomeric cytochrome *c* containing three hemes. The hemes presents bis-histidinyl axial iron coordination and low reduction potentials (Ambler 1991). The triheme cytochrome c_7 has been proposed to have a role in the reduction of iron(III) and manganese(IV) (Roden & Lovley 1993), as also in the sulfur metabolism (Pereira et al. 1997).

The structure of cytochrome c_7 (figure 1.3) is homologous to the tetraheme cytochrome c_3 from *Desulfovibrio* species with the difference that the heme II is absent in cytochrome c_7.

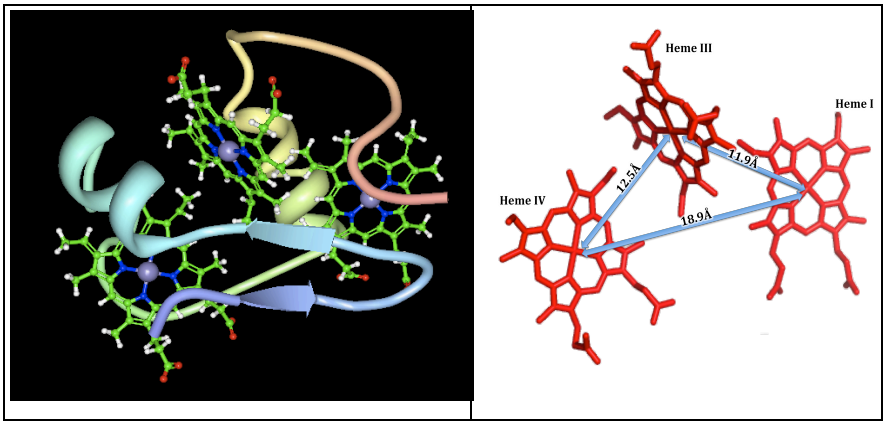

Figure 1.3 – Structure and distance metrics of fully reduced *D. acetoxidans* cytochrome c_7 (Assfalg *et al.* 2002).

Thermal denaturation studies shows that at 20 ^{0}C, cytochrome c_7 is a monomer (Giudici-Orticoni et al. 2003). The thermodynamic parameters of cytochrome c_7 have been

previously determined (Correia *et al.* 2002), which shows that all hemes presents similar microscopic reduction potentials in the physiological pH range (6.0 to 8.0).

It was shown that several aerobic and anaerobic chromium(VI) reducers are able to use organic contaminants as electron donors for chromium(VI) reduction, pointing for treatment of mixed wastes (Lovley & Coates 1997). Assfalg and colleagues revealed that cytochrome c_7 performs the reduction of chromium(VI) showing the presence of a specific binding site for the metal ion. The structure shows that the oxidized chromium(III) binds closer to heme IV than to the other hemes in cytochrome c_7. Heme IV has the highest reduction potential and represent the electron sink for the electrons to be transferred to chromium(VI) (Assfalg et al. 2002). These studies support the notion that cytochrome c_7 displays metal reductase activity, being an accessible tool for remediation of water and soils contaminated by heavy metals.

Its lack of specificity for electron acceptors owed to the low reduction potential of cytochrome c_7 and to the exposure of the hemes (Pereira *et al.* 1997, Correia *et al.* 2002) makes cytochrome c_7 an interesting protein for varied application.

Knowing the thermodynamic parameters of cytochrome c_7, the kinetic reduction behaviour and the putative binding site for metal ions, it is of interest to study the kinetic oxidation behaviour of this cytochrome. This work will focus on detailed molecular mechanism of reduction of metal complexes by cytochrome c_7.

1.2 Electron transfer

1.2.1 Marcus Theory

For one-electron reactions, the theoretical basis for the electron-transfer (ET) kinetics is well developed. In 1954, Marcus developed a model based on a molecular description of ET between small molecules in solution (Marcus 1956). The Marcus theory of electron transfer is widely applied. Long-range electron transfer is an essential component of biological systems, playing an important role in respiration (Marcus & Sutin 1985).

Applicable to interprotein electron transfer, the rates (equation 1.1) of nonadiabatic electron-transfer reactions are controlled by the driving force, reorganization energy, distance between the redox centers, and the nature of the intervening medium separating the electron donor and acceptor.

$$k_{ET} = \frac{2\pi}{\hbar}\left|H_{AB}\right|^2 \frac{1}{\sqrt{4\pi\lambda k_b T}} \exp\left(-\frac{\left(\lambda + \Delta G^0\right)^2}{4\lambda k_b T}\right)$$

Equation 1.1 - Marcus equation (Marcus & Sutin 1985)

In a simple intramolecular system, k will decrease with distance. ΔG^0 is the standard free energy of the reaction, which is related to the standard reduction potentials of the donor D and the acceptor A according to $\Delta G^0 = F(E^0_D - E^0_A)$. The parameter λ, is the reorganization energy, representing the molecular rearrangements that accompany the transfer (both the geometries of the molecules that are oxidized or reduced

and the polarization of the surrounding solvent should be considered). The transmission coefficient, is close to unity for an adiabatic reaction and less than unity (sometimes much less than) for a nonadiabatic reaction (Simonneaux & Bondon 2005).

The pre-exponential term depends on the strength of the electronic coupling (H_{AB}) between the acceptor and the donor. Therefore, pre-exponential term will depend on the overlap of the molecular wave functions of D and A, and therefore on the nature of the redox centers, on their distance, and on the intervening medium.

1.2.2 Thermodynamic and Kinetic modelling

In this work, a kinetic model that makes use of thermodynamic parameters (Catarino & Turner 2001) will be used to discriminate the reference rate constants for each heme in triheme cytochrome c_7 for the oxidation process with metal complexes. The microscopic and macroscopic thermodynamic properties of cytochromes can be assigned by NMR redox titrations at various pH values (Louro *et al.* 1997).

The thermodynamic parameters and the reference rate constants of each heme for the reduction process with sodium dithionite have been determinated in previous work (Correia *et al.* 2002).

Figure 1.4 illustrates the kinetic model for the triheme cytochrome c_7. The pH dependence of the reduction potentials

is a result of the interaction between each heme and the ionisable centre.

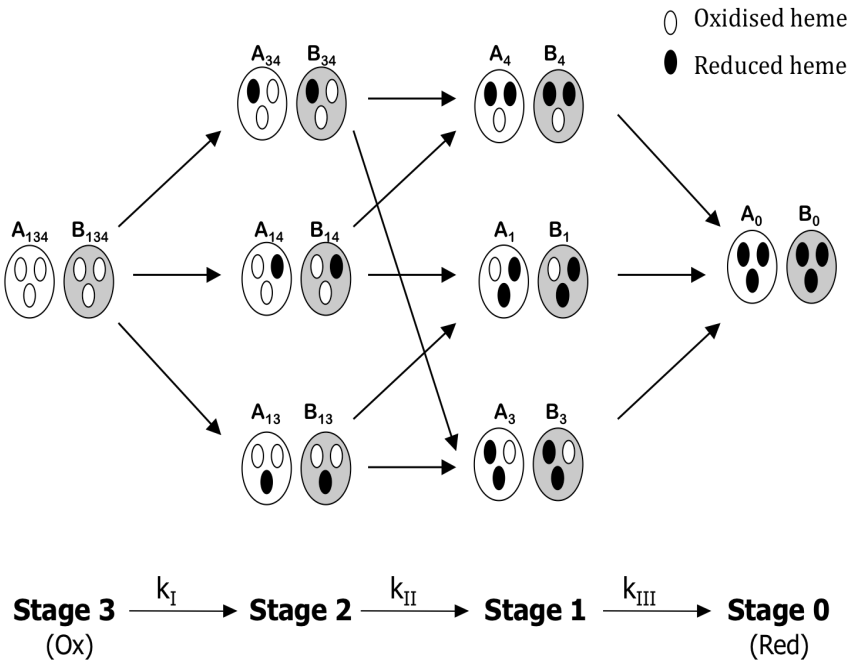

Figure 1.4 – Schematic representation of the microstates of a protein with 3 redox centres and one acid-base centre. A and B represents the protonated and deprotonated microstates respectively. Adapted from (Catarino & Turner 2001).

Cytochrome c_7 may present 8 different redox states from fully reduced to fully oxidised state. Depending on the reduction state of each of the three hemes and on the protonation state of ionisable centre, 16 microscopic states can be defined (figure 1.4). The system involves 8 protonated and 8 deprotonated microstates, which are in fast equilibrium due to the fast proton exchange. After interaction with the redox partner, the 16 microstates can be interconverted through 24 electron transfer microsteps (Correia *et al.* 2002). A microstep is the step between each microstate and it is represented in figure (figure

1.4) by arrows. Each microstate accounts with the ionisable centre, which can be in two states, protonated or deprotonated, so that each arrow represents two possible microsteps.

The kinetic reaction between a protein and a redox partner involves three steps according with scheme 1.1: the complex formation between the redox partner and the protein, the electron transfer reaction between them and the complex dissociation.

$$P^{red} + A^{ox} \underset{k_{-1}}{\overset{k_{+1}}{\rightleftarrows}} [P^{red}\text{-}A^{ox}] \underset{k_{-2}}{\overset{k_{+2}}{\rightleftarrows}} [P^{ox}\text{-}A^{red}] \underset{k_{-3}}{\overset{k_{+3}}{\rightleftarrows}} P^{ox} + A^{red}$$

Scheme 1.1

Considering the multicentre cytochrome c_7, which needs three electrons to be fully reduced, the scheme 1.1 should be considered for each individual centre. Therefore, at least 6 rate constants for each heme for the deprotonated and protonated state are necessary for each microstep, turning the kinetic analysis very complex with a total of 24 rate constants (Correia *et al.* 2002).

On the other hand, in steady state conditions for the protein acceptor complex this scheme can be approximated to a simple collisional model (scheme 1.2) (Capeillere-Blandin *et al.* 1986, De Francesco *et al.* 1994), where the electron transfer is rate limiting, and there is fast equilibrium in the complex association and dissociation.

$$P^{red} + A^{ox} \underset{k_-}{\overset{k_+}{\rightleftharpoons}} P^{ox} + A^{red}$$

Scheme 1.2

Therefore k_+ and k_- are the product of the equilibrium binding constant and the rate constant for electron transfer. The use of large excess of oxidizing agent and the high reduction potential of the oxidizing agent allows further simplification in this system by guaranteeing irreversible electron transfer and pseudo-first order conditions (scheme 1.3).

$$P^{red} + A^{ox} \xrightarrow{k_+} P^{ox} + A^{red}$$

Scheme 1.3

The equations for the rate constants used in the model are analytical, whereas considering reversible reactions the equations need to be integrated numerically. For a three-centre protein as cytochrome c_7, the k_+ has to be defined for each single electron transfer reaction (Paquete 2006).

Considering fast intramolecular electron exchange within microstates belonging to the same oxidation stage, due to the close proximity of hemes, this complex system collapses into a simple kinetic scheme of 3 consecutive macroscopic one-electron transfer steps (figure 1.4).

Under these conditions the electrons equilibrate inside the molecule, according to the relative reduction potentials of the hemes, before the next reduction step meaning that the distribution of electrons inside the molecule is thermodynamically controlled within each redox stage. k_I, k_{II}

and k_{III} are the macroscopic rate constants of each step, which are the values that define the shape of the kinetic trace (Correia *et al.* 2002). These macroscopic rate constants are a weighted average of the microscopic rate constants of all the microsteps in each stage.

The Marcus theory for one-electron transfer (Marcus & Sutin 1985) can establish the relation between the rate constants of each heme in different microsteps (Catarino & Turner 2001). The rate constant of each microstep depends on the structural factors, on the reorganizational energy (λ) and on the thermodynamic driving force. The driving force is defined by the difference between the reduction potential of the donor and acceptor, which may vary between microsteps due to intrinsic differences in the microscopic reduction potentials of the centers. The kinetic model (Catarino & Turner 2001) considers that the reorganisation energy and the reference rate constant do not change during the electron transfer process. Thereafter, the product of the reference rate constant intrinsic to each heme and an exponential factor gives the rate constant of a particular microstep, k_i^j, according to equation 1.2 derived from Marcus theory (Marcus & Sutin 1985):

$$k_i^j = k_i^0 \exp\left[\frac{e_i^j F}{2RT}\left(1 + \frac{e_i^j F}{\lambda} - \frac{e_A F}{2\lambda}\right)\right]$$

Equation 1.2 – Kinetic model based on Marcus equation.

This exponential factor accounts for the driving force associated with the electron transfer in each microstep, being e_i^j

the reduction potential of centre i for each microstep, and e_A the reduction potential of electron acceptor.

In the present work, several different redox partners were prepared and the corresponding reduction potentials ($e_A = E^0$) were determined. The reorganization energy used was 1eV (Christensen *et al.* 1994). Both e_A and λ are assumed to be constant during the reduction process. This way, the rate constants were assumed to be modulated only by the ΔG_i (the driving force between each center of the protein and the redox partner) and by the reference rate constant, which was determined for each redox center.

The kinetic model has already been applied for the reduction of triheme cytochrome c_7 (Correia *et al.* 2002) and of several tetraheme cytochrome c_3 (Catarino & Turner 2001, Paquete *et al.* 2007) with sodium dithionite.

The present work reports for the first time, the application of the kinetic model for the oxidation of cytochromes, indicating that this model enables the analysis of kinetic properties of systems under thermodynamic control.

1.3 Biorganometallics

Organometallic chemistry and biochemistry have been merged in the last two decades into a new field: biorganometallic chemistry (van Staveren & Metzler-Nolte 2004). To study the oxidation behaviour of cytochrome c_3 and c_7 it is of interest to analyse how the electron transfer occurs using different known mediators. These mediators can be

organometallic compounds, which may have the capability to interact with biomolecules and perform one-electron transfer reactions at different reduction potentials. Ferrocenes and cobalt complexes present these abilities (van Staveren & Metzler-Nolte 2004) (Bailar 1946).

1.3.1 Ferrocenes

The discovery of ferrocene and elucidation of its remarkable structure has been proposed to mark the starting point for modern organometallic chemistry (Stepnicka 2008). The stability of the ferrocenyl group, the accessibility of a large variety of derivatives, and its favourable electrochemical properties have made ferrocene and its derivatives very popular molecules for biological applications with biomolecules (van Staveren & Metzler-Nolte 2004). Iron undergoes a reversible one-electron reduction from Fe(III) to Fe(II). The ferrocenyl group [$Fe(\eta^5\text{-}C_5H_4)(\eta^5\text{-}C_5H_5)$] is herein denoted as Fc and ferrocene [$Fe(\eta^5\text{-}C_5H_5)_2$] as FcH.

Ferrocene is a neutral molecule and is soluble in many common organic solvents. Ferrocene features a reversible one-electron oxidation and in conjugation with the stability of the corresponding ferrocenium salts, ferrocene/ferrocenium is a very stable redox pair (Togni et al. 1995). The reduction potential for the ferrocene/ferrocenium couple depends on the solvent used and is E^o = 0.31V vs. saturated calomel electrode (SCE) in acetonitrile (Long 1998).

In coordination chemistry, the ferrocene moiety has

played a significant role as a backbone or a substituent in ancillary ligands due to the specific and unique geometries that the ferrocene provides, and its electronic (redox) properties. The possibility of switching the redox state of the ferrocene backbone gives potential access to control the reactivity of the metal center. Ferrocene undergoes facile electrophilic substitution, it is sensitive to oxidation and thus reactions such as halogenation and nitration cannot be used for the synthesis of substituted ferrocenes. In fact, only radical substitution and electrophilic substitution under nonoxidising conditions, borylation, lithiation and mercuration can be used for the formation of substituted ferrocenes (Stepnicka 2008).

The oxidation potential of the ferrocene/ferrocenium couple, changes according to the nature and number of substituents. In general, the potential shift depends on the substituent's electron-donating or –accepting power (electrophilicity) (Silva et al. 1994).

1.3.2 Cobalt complexes

Dichlorobis (ethylenediamine) cobalt(III) cation $[Co(en)_2Cl_2]^+$ is a coordination compound where the cobalt contains four ligands (two Cl^- and two "en"). The bonding between the Co^{3+} ion and Cl^- and "en" ligands is via coordinate covalent bonds arranged octahedrally around the metal center (Pearson & Basolo 1956).

Since each "en" ligand is bidentate, two different

geometric isomers of cobalt complex are possible to form, a *cis* form and a *trans* form (figure 1.5).

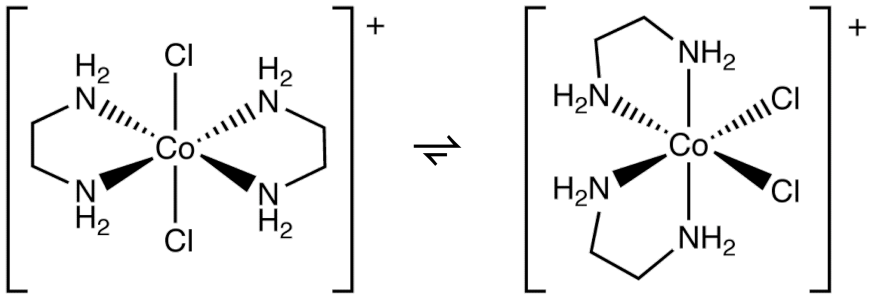

trans-$[Co(en)_2Cl_2]^+$ *cis*-$[Co(en)_2Cl_2]^+$

Figure 1.5 - *Cis-trans* isomerisation of Dichlorobis(ethylenediamine)cobalt(III).

The *cis-trans* interconversion was first discovered by Jorgensen cited in (Niederhoffer *et al.* 1986). Because of the particular splitting of the *d*-orbitals of the Co^{3+} center, the *trans* complex is green and the *cis* complex is purple (Bailar 1946). *trans*-dichlorobis(ethylenediamine)cobalt(III) changes to the *cis* form on heating in water (Haworth et al. 1955). The presence of acid, however, causes the reverse change to take place (Bailar 1936).

Recently, spectroscopic and electrochemical studies have been performed, showing that the *cis* and *trans* complexes presents similar electrochemical characteristics (Vivier et al. 2006).

In this work the two isomers *cis* and *trans* of the coordination compound $[Co(en)_2Cl_2]^+$ will be synthesized.

2 Materials and Methods

2.1 Source of organisms

The type strain *Desulfuromonas acetoxidans* (DSM 684) was purchased from German Collection of Microorganisms and Cell Cultures (DSMZ), Braunchweig, Germany.

2.2 Cell cultivation

Standard anaerobic techniques were used during all the procedures involving bacterial growth (Hungate 1969, Miller & Wolin 1974, Fonseca 2007).

2.2.1 Growth of Stock cultures

To prepare laboratory stock cultures, cells were first cultivated using a modified medium for *D. acetoxidans* described in the Catalogue of Strains of the DSMZ (http://www.dsmz.de/microorganisms/html/strains/strain.dsm000684.html). The medium composition per litre of distilled water, was as follows: NH_4Cl, 20.0g; Na_2SO_4, 0.3g; $MgSO_4.7H_2O$, 1.0g; $MgCl_2.6H_2O$, 2.0g; KH_2PO_4, 1.0g; NaCl, 1.77g; $CaCl2.2H_2O$, 0,1g (all from Fluka); Trace element solution SL-4, 10.0ml [EDTA, 0.500g; $FeSO_4.7H_2O$, 0.200g; $ZnSO_4.7H_2O$, 0.010g; $MnCl_2.4H_2O$, 0.003g; H_3BO_3, 0.030g; $CoCl_2.6H_2O$, 0.020g; $CuCl_2.2H_2O$, 0.001g; $NiCl_2.6H_2O$, 0.002g; $Na_2MoO_4.2H_2O$, 0.003g

(all from Fluka) and Distilled water, 1000ml]. As terminal electron acceptor, disodium fumarate (Fluka) was used and added to the medium to obtain a final concentration of 30mM. In order to remove dissolved oxygen, the media were boiled and cooled down to room temperature under nitrogen atmosphere, for approximately 90min and capped with a thick rubber stopper before autoclaving. Separately, the following supplements were made and added to the deoxygenated and sterilized medium (per litre): 20 μg/ml biotin (Fluka), 1.0 ml; 4.0M HCl (Pronalab), 1.0ml; absolute ethanol (Panreac), 1.0 ml; 0.80M $NaHCO_3$ (Sigma), 60.0 ml; 0.07M $Na_2.9H_2O$ (Sigma), 20.0 ml. The $NaHCO_3$ and $Na_2S.9H_2O$ supplements were deoxygenating for about 90min and then sterilized by autoclaving at 121ºC during 30min. 4.0M HCl was added to obtain a final pH of 7.2.

Cellular growth was initiated with 20% inocula. The cells were grown in the dark, without stirring, at 30ºC for 24 hours. The cultures were stored at 4ºC for later use in growth, and at -80ºC after addition of glycerol (10%) to the culture for long-term preservation.

2.2.2 Cellular growth using Fumarate as the terminal electron acceptor

In a procedure similar to that used for the preparation of stock cultures, fumarate was used as terminal electron acceptor

during the initial steps of scale-up. Ethanol was used as carbon source and as electron donor.

2.2.3 Cellular growth using Sulphur as the terminal electron acceptor

At the last step of each scale-up the terminal electron acceptor used was elemental Sulphur (Fluka) instead of Fumarate, to a final concentration of 60mM (2 grams per litre of medium). For the medium containing elemental sulphur the autoclaving conditions were changed to 110 ^{o}C during 60 min to avoid melting of the sulphur. In this case the deoxygenation of the media was performed after autoclaving, under nitrogen flow during 120min, using a connection into the bioreactor (10.0l). The carbon source and electron donor was ethanol. Bacterial growth was initiated with the previous 1500ml basal medium fumarate/ethanol matching a 20% inoculum volume. The cells were grown for 48 hours at 30º C in the dark without stirring in a procedure similar to the previous steps.

2.2.4 Large scale cell cultivation

In order to obtain sufficient biomass for the purification of proteins, large-scale growth batches of *D. acetoxidans* DSM 684 were performed. Scale-up was performed using the media and conditions previously described.

Large-scale growth batches of 16 litres (2 x 8 litres simultaneously) were run until the culture reached roughly the

late-log stage of growth (OD = 0.8). To avoid the catabolic turn off and degradation of terminal reductases, bacterial growth was always stopped before it entered the stationary phase i.e. after each 24 hours/batch (Fumarate as terminal electron acceptor) and 48 hours/batch (Sulphur as terminal electron acceptor) (Fonseca 2007).

2.3 Protein Purification

2.3.1 Cell harvest and disruption

Prior to cell harvest, the precipitates in the culture owing to unreacted elemental sulphur were removed through decantation. Decanted cells were harvest by centrifugation at 11300 g for 15 min at 4 ^{0}C (Beckman J2-21M/E centrifuge). The biomass obtained from all growths was collected, washed with 10mM Tris-HCl (pH7.6) buffer and centrifuged at 11300 g for 15 min at 4 ^{0}C.

Prior to cellular lysis, the cellular pellet was resuspended in 10mM Tris-HCl (pH7.6) buffer containing deoxyribonulease (Sigma) and a tablet of protease inhibitors cocktail (Sigma). Cellular lysis was performed in a French Press (three times at 1000 Psi) (Termo Scientific®) using a fast-flow anaerobic kit (figure 2.1). The disrupted cell lysate was collected and maintained at 4ºC.

Figure 2.1 – French-Press equipment in use with fast-flow anaerobic kit assembled

2.3.2 Separation of soluble from membrane fractions

The collected cell lysate was centrifuged at 11300 g for 15 min at 4 ^{0}C) and the supernatant (crude extract) retained. The supernatant was then ultracentrifuged at 22000 g for 90 min at 4 ^{0}C (Beckman Coulter Optima™ LE-80K Ultracentrifuge) to separate the soluble protein fraction from the membrane fraction. The pellet (membrane fraction) was stored for future work, and the supernatant (soluble fraction) was dialysed against 20mM Tris-HCl pH 7.6 buffer at 4ºC overnight.

2.3.3 Protein purification

After dialysis, the soluble fraction was fractionated on a DEAE Sepharose Fast-Flow anion exchange column (Amersham Pharmacia Biotech®) equilibrated with 20mM Tris-NaCl buffer pH 7.6. The column was washed with the same buffer to remove

unabsorbed proteins and eluted with a linear gradient of 0-1M NaCl in 20mM Tris-HCl buffer pH 7.6 at a flow rate of 6ml/min. Red fractions were concentrated by ultrafiltration on an Amicon® diaflo with a cut-off membrane of 3000 Dalton (Millipore®). Those containing a 9kDa band with purity index (A_{409}/A_{280}) greater than 1.0 were pooled, dialyzed against 20mM Phosphate (pH 7.6) buffer and the desalted solution was centrifuged at 15000g for 20 min at 4 ^{0}C. The resulting sample (approximately 15ml) was loaded on a HTP column (Amersham Pharmacia Biotech®) previously equilibrated with 20mM Phosphate pH 7.6 and eluted with a linear gradient of 0-1M Phosphate buffer pH 7.6 at a flow rate of 3ml/min. Previous work shows that the cytochrome c_7 tends to precipitate slowly when stored frozen in 10mM Tris buffer (Probst et al. 1977). To prevent this, it was used 100mM Tris buffer (pH7.6). Fractions were checked for purity by SDS-PAGE, UV-Visible spectroscopy and NMR spectroscopy.

2.3.4 UV-Visible spectroscopy

The absorption and emission of electromagnetic radiation of specific energy (wavelength) is a characteristic feature of many molecules, as a consequence of the promotion of electrons to excited electronic states, in accordance with the laws of quantum mechanics.

UV-Visible spectrophotometry is a useful technique for identification of metalloproteins. It is based on two fundamental principles were the absorption of light is exponentially related:

to the solute concentration I and to the length of the light path through the absorbing solution (*l*). The absorbance (*A*) is a logarithmic relation between the intensity of incident light (I_0) and the emergent light (*I*), represented in the Beer-Lambert relationship where ε is a constant absorption coefficient of the solute:

$$A = \log_{10}\left(\frac{I_0}{I}\right) = \varepsilon l C$$

Equation 2.1 Beer-Lambert law.

The known absorption characteristics of heme-proteins allow the identification of type of heme, the spin and the oxidation state through characteristic bands represent on the visible spectra.

Cytochromes have UV-visible spectra with three characteristic bands, α and β bands between 600-500nm and the *Soret* band between 430-390 nm. The distinctive wavelengths for each of these bands can be used to classify the present cytochrome (Moore & Pettigrew 1990).

A broad band between 600-500 nm, and a *Soret* band between 430-390 nm characterize the oxidized state of cytochromes. In the reduced form the *Soret* band is shifted to higher wavelengths and the α and β band become sharper (Catarino 1998).

2.3.5 NMR spectroscopy

Nuclear magnetic resonance spectroscopy is based on differences in energy of the magnetic states of atomic nuclei, placed in an external magnetic field. The effective field at the nucleus is the difference between the magnetic field (B_0) and its product by shielding constant (σ). The shielding constant (σ) expresses the contribution of the small secondary field generated by the nearby electrons in the molecule. The magnitude of σ depends on the electronic environment of a nucleus, so nuclei of the same isotope give rise to small different resonance frequencies. The separation of resonance frequencies resulting from the different electronic environments of the nucleus of the isotope is called the *chemical shift (*δ) (Levitt 2001).

In frequency units the chemical shift is proportional to the applied static magnetic field, and therefore chemical shifts are customarily quoted in *parts per million* (ppm) units expressed against an internal standard (Wuthrich 1986).

2.3.5.1 Sample preparation

The sample used for NMR studies was dialyzed against twice-distilled water and then lyophilized three times in 99.9% D_2O to reduce the water signal and to exchange the labile protons. The NMR tubes were prepared under aerobic conditions and, consequently, the samples were obtained in the

oxidized form, since the hemes have very low reduction potentials.

2.3.5.2 NMR spectroscopy

One-dimensional ^{1}H-NMR spectra were acquired on a Bruker AMX-300 spectrometer (magnetic field strength 7.058 T, 300 MHz for proton resonance frequency). 256 scans were done, the spectral width was 240Hz and the data was smoothed with a exponential window function with a line broadening (LB) of 10Hz. The temperature of the sample was kept at 303 ± 1.0 K.

2.4 Ferrocenium sample preparation

For kinetic experiments ferrocenium cations were required as oxidant agents. Mono-substituted ferrocenia were prepared by one-electron oxidation of each mono-substituted ferrocenes. Ferrocene monocarboxylic acid, ferrocenylacetic acid and α-hydroxyethyl ferrocene were purchased from Strem®. Ferrocenylethanol was synthesized following a modified method (described on section 2.4.1) from Davis and colleagues (2005) and recrystallized as described by Rinehart and colleagues (1957).

Ferrocenes are insoluble in protic solvents and soluble in most organic solvents (Stepnicka 2008). For experimental tests, ferrocene had to be prepared in the same aqueous solution used on thermodynamic and kinetic studies of cytochrome c_7

reported in the literature (Correia *et al.* 2002). Stock solutions of 10mM of each ferrocene were prepared by initial dilution on 200.0µl of absolute ethanol to a final volume of 1.0ml of tris-maleate buffer at pH 6.0, 7.0 and 8.0.

2.4.1 Ferrocene synthesis: 2-Ferrocenylethanol

The synthesis of 2-ferrocenylethanol was achieved by the reduction of 2-ferrocenylacetic acid using $LiAlH_4$ as a reducing agent. A Schlenk flask with $LiAlH_4$ was carefully connected to a flask under nitrogen pressure, and sufficient $LiAlH_4$ to ensure excess of reducing agent was added (318.0mg, 8.3mmol) and suspended in dry ether (15.0cm^3). Ferrocenylacetic acid (250.0mg, 1.0mmol) in dry ether (5.0cm^3) was slowly added (drop by drop) to the $LiAlH_4$ suspension while slight boiling was maintained (Davis et al. 2005).

LiAlH4 is a dangerous reagent that violently reacts with water including atmospheric moisture. The mixture was refluxed for 13 h at 50.0 ºC with two overnight breaks (2 hours + 8 hours + 2 hours) just maintaining the stirring.

Subsequently an 1:1 ethanol:ether mixture (10cm^3) was very carefully added to destroy the excess $LiAlH_4$. The reaction mixture was slowly poured into excess of ice-cold 2 M NaOH solution (150.0cm^3) and the ether and aqueous phases separated. The aqueous phase was washed with ether after which the ether fraction was washed with 1 M NaOH (50.0cm^3) and twice with equal volumes of water. This procedure dissolves the remaining COOH and solubilises Al^{+3} and Li^{+1} with

hydroxyls that will be in water phase. In order to dry the ether layer, $MgSO_4$ was added and the solvent removed under reduced pressure. The solution was dried on a rotary evaporator (Davis et al. 2005).

To improve the purity of the product, recrystallization was performed. A mixture of ether-pentane (both with a 36 ^{0}C boiling point) was used to dissolve the remaining residues, and ferrocenylethanol recrystallized in ether. The flask was cooled on a freezer (-20 ^{0}C) for 2 hours. (Rinehart Jr et al. 1957)

2.4.2 NMR Spectroscopy of ferrocenes

NMR analyses of ferrocenylethanol and its precursor ferrocenylacetic acid were performed on a Bruker Avance III 400 NMR spectrometer using $CDCl_3$ as solvent.

2.4.3 Ferrocene oxidation

To perform a one-electron oxidation of cytochrome c_7, ferrocene mediators had to be oxidized previously to respective ferrocenium derivatives. To avoid the presence of unwanted chemical substances, oxidation was performed electrochemically with a potentiostat (Autolab® PSTAT10) achieving equal spectra as chemical oxidation. A potential above the $E^o_{1/2}$ of each ferrocene was imposed until a complete oxidation state was achieved. The oxidation procedure was followed by amperometry, which measures the intensity of the current, which becomes near zero after complete oxidation of ferrocenes.

2.4.4 Voltammetry studies

Evaluation of standard electrode potentials of ferrocenes performed by different workgroups should be taken with the appropriate care because each group mentions their reduction potential versus different reference electrodes. IUPAC recommends the use the FcH/FcH^+ couple as an internal standard (Ives et al. 1961). Herein, aqueous solutions will be used for all kinetic experiments, an hence standard electrode potentials will be reported versus the conventional reference electrode standard hydrogen electrode (SHE). In practical laboratory measurements, a secondary reference electrode is used, a reference whose potential *vs* SHE (aq) is well known, +0.241 for the (KCl) saturated calomel electrode (SCE), +0.197 for the saturated silver/silver chloride electrode, +0.209 for 3M NaCl silver/silver chloride electrode, all at 25 ^{0}C (Ives et al. 1961) (Zoski 2007).

Cyclic voltammetry was performed using an Autolab® PSTAT10 electrochemical analyser. A three-electrode configuration was used in a cuvette-cell, specially designed to work with a micro magnetic stirrer. A platinum wire was used as the counter electrode and the reference electrode was a standard $Ag^+/AgCl$ electrode. Scan rates between 50 and 150mV/s were tested to identify the best conditions for each ferrocene. Data were collected at room temperature before and after the oxidation procedure.

2.4.5 UV-Visible spectroscopy

The reduced and oxidized state of each ferrocene was checked by UV/Visible spectroscopy. The different spectra allow the characterization of ferrocene oxidation state. All spectrometry experiments were performed on a Shimadzu UV-3100 spectrophotometer.

2.5 Sample preparation of Cobalt complexes

2.5.1 *Trans*-dichlrobis(ethylenediamine)cobalt(III)

The *trans*-dichlorobis(ethylenediamine)cobalt(III) *trans*-$[Co(en)_2Cl_2]^+$ was prepared as described by Bailar (Bailar 1953) at room temperature.

A glass beaker large enough to contain a 100ml Erlenmeyer flask was used as water bath on a hot plate. The water bath was heated just below the boiling point (with addition of additional water to the bath as needed, to account for evaporation). A 10ml portion of MilliQ water (Millipore) was added to 4 g of $CoCl_2.6H_2O$. After dissolution 15ml of a 10% solution of ethylenediamine was added to the mixture. The mixture was stirred over the steam bath during 40 minutes, maintaining the bath volume by adding small volumes of water. During this process, the $Co^{2+}$is oxidized to Co^{3+} by the oxygen in the air and the ethylenediamine ligands are coordinating to the metal (Bailar 1953). Good stirring is necessary to promote solvation of the oxygen.

After the oxidation, 12mL of concentrated 12M HCl was

added maintaining the heating and stirring, without addition of water, until a thin slurry of crystals has formed. The slurry was cooled to room temperature stirring occasionally for 15 minutes. The mixture was filtered and washed with 5mL of 6M HCl obtaining a pure green product. The final product was dryed and weighted.

2.5.2 *Cis*-dichlrobis(ethylenediamine)cobalt(III)

The *cis*-$[Co(en)_2Cl_2]^+$ was synthesized from the *trans*-$[Co(en)_2Cl_2]^+$ compound (Haworth et al. 1955). A 50mg portion of *trans*-$[Co(en)_2Cl_2]^+$ complex was dissolved in 20ml of distilled water and gently evaporated while the solution was heated at 100ºC. This procedure was repeated three times. The residual product was then mixed with very cold water (Vivier et al. 2006).

2.5.3 Voltammetry studies

Cyclic voltammetry was performed as described on section 2.4.4.

2.5.4 UV-Visible spectroscopy

UV-visible spectroscopy was followed as described on section 2.4.5.

2.6 Kinetic Studies

Kinetic reactions between the cytochrome c_7 and all the ferrocenium cations were followed by stopped-flow assay using HI-TECH Scientific® Stopped-Flow equipment (SF-61DX2), working on single mix mode. The Stopped-flow equipment works inside an anaerobic glove-box (Mbraun MB150-GI) (figure 2.2). The data were acquired using a wavelength of 552nm, and 512 points per second were registered ensuring accuracy in the measurement of fast kinetic reactions. The data collected were analysed with HI-TECH Scientific Kinetic Studio.

Figure 2.2 – Stopped-flow equipment.

For light calibration, the input Xenon light intensity (As LPU 150 Xenon lamp) was set according to a standard operating procedure defined by the manufacturer.

2.6.1 Circuit washing

The SAMPLE HANDLING UNIT circuit is coated with Teflon and because of its permeability to oxygen and dithionite,

all the circuit has to be washed according to a standard operating procedure defined by the manufacturer. Prior to each experiment the circuit was washed using a 2M solution of H_2SO_4 during 15 minutes followed by a 4M solution of NaOH during 15 minutes and finally washed abundantly with distilled water.

2.6.2 Circuit refill procedure

The volume of the stop syringe was set up to 100μL and the circuit has a volume near 40μL. To make sure that all the circuit of the SAMPLE HANDLING UNIT was filled with the corrected solutions, it was necessary to make at least three single shots before data acquisition.

2.6.3 Dead time calculation

In kinetic studies by the method of stopped-flow, the dead time (t_d) of the instrument is the time between the end of mixing the two solutions and the beginning of observation of the kinetics of the reaction.

Calculation of t_d is crucial to know the performance of the stopped-flow instrument and it depends on the distance between the mixer and the cell, the final velocity of the flow at the instant the flow is stopped, the efficiency of the mixer and the viscosity of solutions.

T_d was calculated through the 2,6-dichlorophenolindophenol reduction with L-ascorbic acid (Matsumura et al. 1990), studying this first-order reaction in which the concentration of a coloured solution of (DCPIP) falls

to zero after mixing with a decolorizing solution (Ascorbic Acid). The transmission of light was calibrated with distilled water and the wavelength was set to 524nm. Table 2.1 lists the solutions used.

Table 2.1 – Ascorbic acid *versus* DCPIP solution preparation

	Solution	Preparation
A	0.2mM DCPIP	6 mg DCPIP / 50 ml H_2O
B_6	100mM Ascorbic acid, 20mM HCl	500mg Ascorbic acid/25ml C
B_5	50mM Ascorbic acid, 20mM HCl	5 ml B_6 + 5 ml C
B_4	20mM Ascorbic acid, 20mM HCl	2 ml B_6 + 8 ml C
B_3	10mM Ascorbic acid, 20mM HCl	1 ml B_6 + 9 ml C
B_2	5mM Ascorbic acid, 20mM HCl	0.5 ml B_6 + 9.5 ml C
B_1	1mM Ascorbic acid, 20mM HCl	0.1 ml B_6 + 9.9 ml C
C	20mM HCl	331.2µL HCl 37%/200ml H_2O

Syringes were first filled with solutions A and C and a sequence of three single shots were done, to acquire the absorbance value of DCPIP. Subsequently, solution C was replaced with solutions B_1 to B_6 making three single shots in each assay. Between each experiment, the refill and shot procedure was done as described on 2.6.2, ensuring a complete exchange of solutions on the Stopped-flow circuit. The acquisition time was adjusted to 0.1 seconds. The data collected were treated converting the absorption values into reduced fraction. Figure 2.3 gives an example of a kinetic trace taken with the stopped-flow instrument.

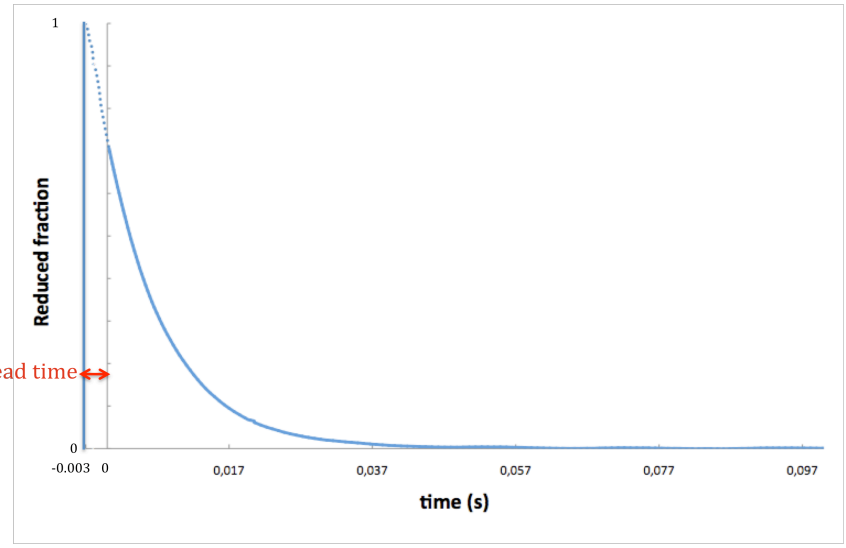

Figure 2.3 – Cartoon of dead time determination.

The first milliseconds in which the reaction returns no measurable data represented in figure 2.3 are the dead time.

2.6.4 Experimental assay

The traces were acquired at 552nm and the temperature maintained at 289.0 ± 1.0K, the same conditions used in the study for the thermodynamic and reduction kinetics of cytochrome c_7 (Correia et al. 2002). Stock solutions of buffers were prepared inside the anaerobic glove box with a final concentration of 100mM Tris-maleate, 400mM KCl at pH 6.0, 7.0 and 8.0.

2.6.4.1 Light calibration and circuit refill

The transmission of light was calibrated with 100mM Tris-maleate at pH 6.0, 7.0 and 8.0 with ionic strength set to 500mM trough addiction of KCl.

2.6.4.2 Preparation of mono-substituted ferrocenes

The preparation of all the mono-substituted ferrocene samples was made from dilution of previous stock solutions. After electrochemical oxidation of ferrocenes to ferrocenium, the solutions were deoxigenated with cycles of argon and vacuum. To ensure a concentration of 100μM after-mixing, solutions of 200μM concentration before-mixing were prepared for each ferrocene using the three buffer solutions of 100mM Tris-maleate, 400mM KCl, at a final pH of 6.0, 7.0 and 8.0.

2.6.4.3 Sodium dithionite sample preparation

The reduced state of the cytochromes was achieved using sodium dithionite as reducing agent, recrystallized previously in order to obtain 95% pure material (Paquete 2006). Solid sodium dithionite was added to Tris-maleate buffer 100mM at pH 8.0 with ionic strength set to 500mM by addition of KCl. The concentration of reducing agent was measured by UV-visible spectroscopy using ε_{314} = 8000 $M^{-1}cm^{-1}$ (Dixon 1971). All the procedures were performed inside the anaerobic chamber.

2.6.4.4 Preparation of cytochromes samples

For the optimization of the experimental procedure a solution of the tetraheme cytochrome c_3 from *D. gigas* was used. The triheme cytochrome c_7 purified as described on section 2.3 was used for kinetic experiments. Cytochromes were degassed with cycles of argon and vacuum (three cycles each one of 5

min). A few microlitres of reducing agent sodium dithionite solution were added to reduce the cytochrome. After cytochrome reduction, the excess of dithionite was removed with an Amersham Biosciences PD-10 desalting column. Desalted cytochrome was diluted in buffer solutions of 100mM Tris-maleate at pH 6.0, 7.0 and 8.0 inside an anaerobic chamber under an argon atmosphere with O_2 level lower than 0.8ppm. The ionic strength was set to 500mM through the addition of KCl. UV-visible spectroscopy was used to measure the concentration of cytochrome c_3 using ε_{552} = 120000 $M^{-1}cm^{-1}$ (Moura unpublished), cytochrome c_7 using ε_{552} = 90000 $M^{-1}cm^{-1}$ (Correia et al. 2002) and sodium dithionite using ε_{314} = 8.000 $M^{-1}cm^{-1}$ (Dixon 1971).

2.6.5 Kinetic Modelling

The stopped-flow kinetic data were fitted taking in account the dead time calculated in section 2.6.3. The absorption of the kinetic traces was converted into reduced fraction.

The kinetic model was fit to the kinetic data simultaneously with the known thermodynamic parameters (Correia *et al.* 2002) using the Nelder-Mead simplex algorithm implemented in MATLAB (The MathWorks) (Lagarias *et al.* 1998).

3 Results

3.1 Bacterial growth

Figure 3.1 shows the scale-up procedure (represented in duplicate) from the 10 ml initial stock culture until the final 8000 ml of growth. After 24 hours of growth, a vivid red colour was observed.

Figure 3.1 – Scale-up procedure for large-scale growth of *D. acetoxidans*. The terminal electron acceptor was fumarate at the initial steps and sulphur at the final step. Ethanol was used as carbon/electron donor.

Scale-up procedure was done in duplicate, achieving 16 litres grown culture at the end of each one. Four duplicate scale-up growths were prepared reaching 64 litres of final culture volume, obtaining 82.0 grams of biomass representing a yield of 1.3 grams of biomass/litre of medium.

3.2 Protein Purification

The crude cell extract was obtained by French-pressure lysis and the soluble extract separated by centrifugation. The soluble extract was loaded on a DEAE anionic column followed by an HTP column. Figure 3.2 illustrates the purification scheme followed in this work.

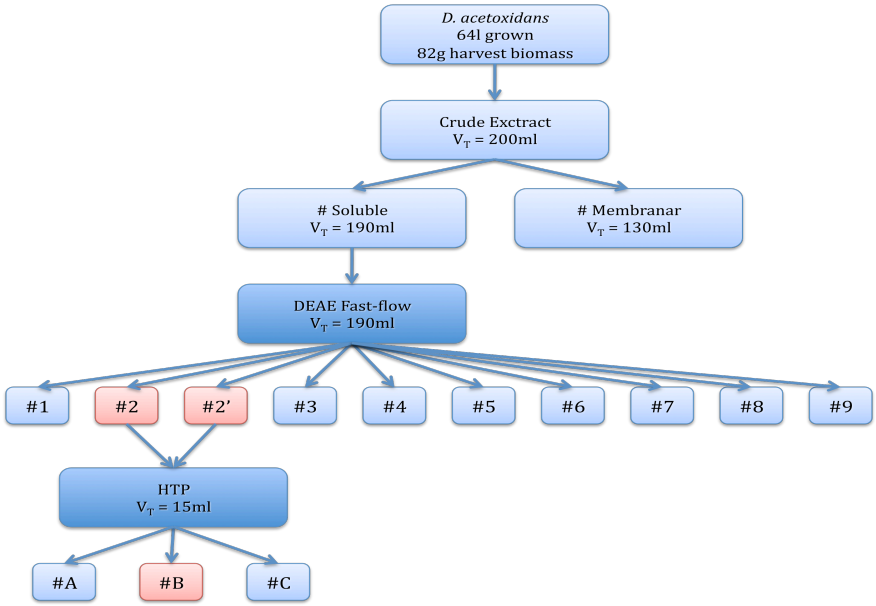

Figure 3.2 - Schematic representation of protein purification.

Ten fractions were obtained from the DEAE anionic column and concentrated by ultrafiltration through an Amicon diaflo. Aliquots from each fraction were used to perform a SDS-PAGE, represented on figure 3.3. The fraction #9 was not placed in the gel because the cytochrome c_7 elutes at low ionic strengths (Probst et al. 1977).

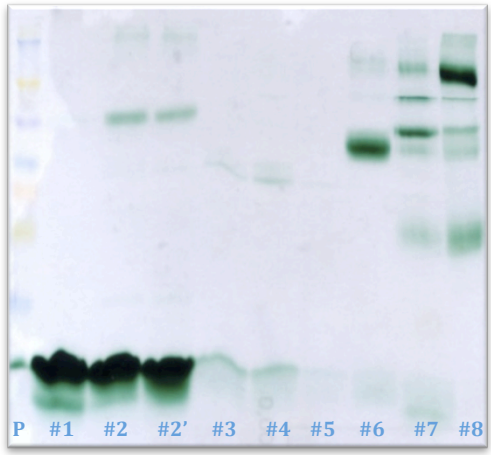

Figure 3.3 – SDS-PAGE haem staining

UV/Visible spectroscopy of each fraction was measured (figure 3.4) in the range of 800 nm to 250 nm.

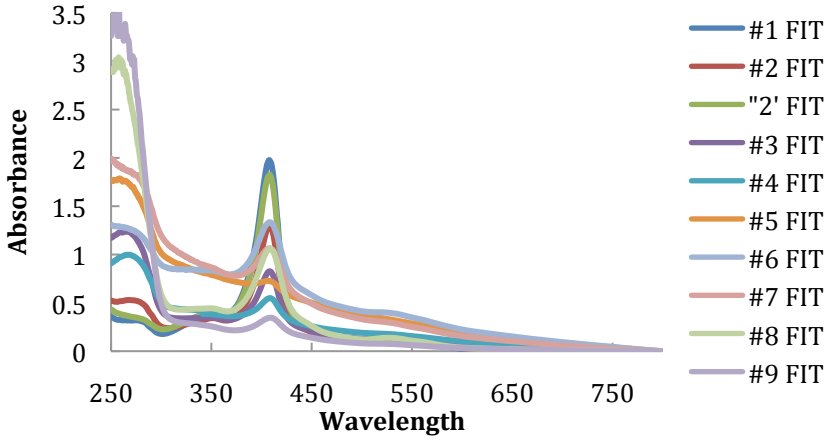

Figure 3.4 –UV-Visible DEAE Fractions Spectra.

The absorbance values at 280 nm and 408 nm were registered (table 3.1) and the absorbance ratio ($A_{408/280}$) was calculated to estimate the cytochrome purity level of each fraction.

Table 3.1 – Absorbance values at 280nm and 408nm of each fraction from DEAE column.

Fraction	Volume (ml)	A_{280}	A_{408}	Ratio
# 1	10.0	0.326	1.990	6.10
# 2	16.0	0.524	1.318	2.52
# 2'	4.0	0.409	1.898	4.64
# 3	9.0	1.192	0.939	0.79
# 4	15.0	1.100	0.734	0.67
# 5	9.0	1.938	1.119	0.58
# 6	7.0	1.679	1.823	1.09
# 7	8.0	2.091	1.393	0.67
# 8	25.0	1.943	1.086	0.56
# 9	11.0	2.298	0.395	0.17

Fraction #1 from DEAE separation presumably contains cytochrome but was stored for future purification. The fractions #2 and #2´ were collected and loaded on a HTP column, obtaining 3 fractions #A, #B and #C. Aliquots from each fraction were used to perform a SDS-PAGE gel (figure 3.5).

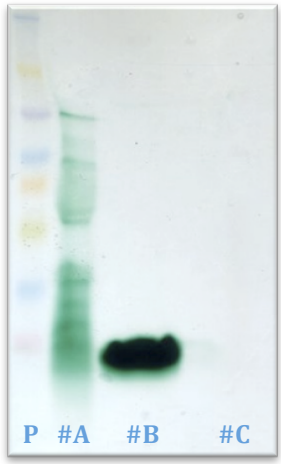

Figure 3.5 – SDS-PAGE haem staining

UV/Visible spectroscopy of fraction B obtained from HTP column was done in the range 800 - 250 nm (figure 3.6)

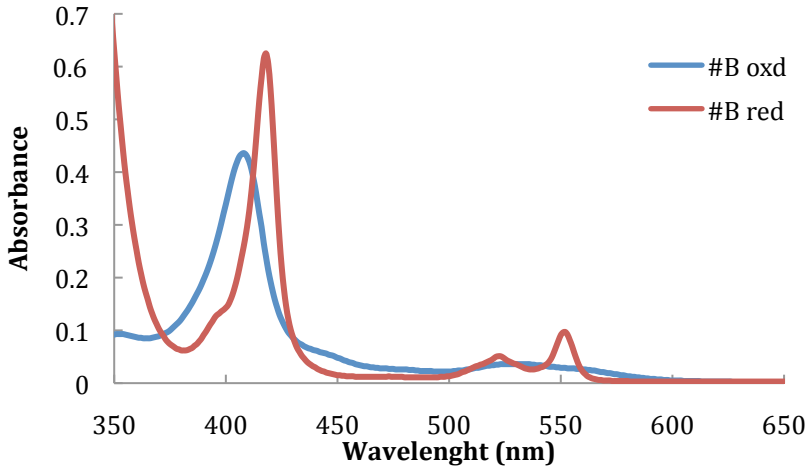

Figure 3.6 –UV-Visible fraction B spectra from HTP column separation diluted 250x.

The fraction B was concentrated to 600µl NMR tube and SDS-PAGE was prepared to confirm a pure protein near 9000 Dalton and its spectrum shows an absorbance ratio $A_{408/280}$ = 11.18 representing high purity achieved.

According to Beer-Lambert law, and using the cytochrome c_7 ε_{552} = 90000 $M^{-1}cm^{-1}$ the calculated concentration of cytochrome c_7 was 2.48mg/ml, which represents a total of 1.49mg in the NMR volume obtained.

3.3 NMR spectroscopy of protein

NMR spectroscopy was performed for identification of cytochrome c_7 in its oxidized form, which was characterized by some signals of heme substituents shifted to high frequency. The majority of the resonances of the heme methyls appear isolated from the other signals of the heme substituents.

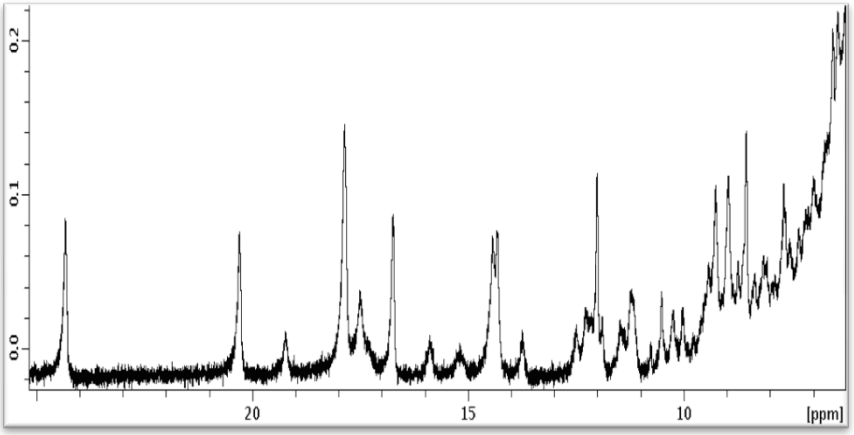

Figure 3.7 – ^{1}H-NMR spectrum of purified cytochrome c_7 with 256 scans at 303.0 ± 5.0 K on a Bruker AMX 300MHz spectrometer.

The spectrum of purified cytochrome represented in figure 3.7 is similar to those found in the literature (Moura *et al.* 1984,

Correia *et al.* 2002). The cytochrome c_7 was successfully purified.

3.4 Ferrocene as mediator

3.4.1 Ferrocenylethanol synthesis

Ferrocenylethanol was synthesised as described on section 2.4.1. Figure 3.8 represents the synthesis process to get the final reddish-brown oil (Davis et al. 2005).

Figure 3.8 - Ferrocenylethanol synthesis.

The synthesis was performed from reduction of 250.0mg of Ferrocenylacetic acid. 10mg of Ferrocenylethanol were obtained which represents a yield of 4%.

3.4.2 NMR spectroscopy of ferrocenes

NMR analyses of ferrocenylethanol and its precursor ferrocenylacetic acid were done to certify the purity of the synthesized ferrocenylethanol and check if the initial compound is still present. The spectrum of ferrocenylacetic acid represented in figure 3.9 shows high similarity with previous publications for this compound (Davis et al. 2005).

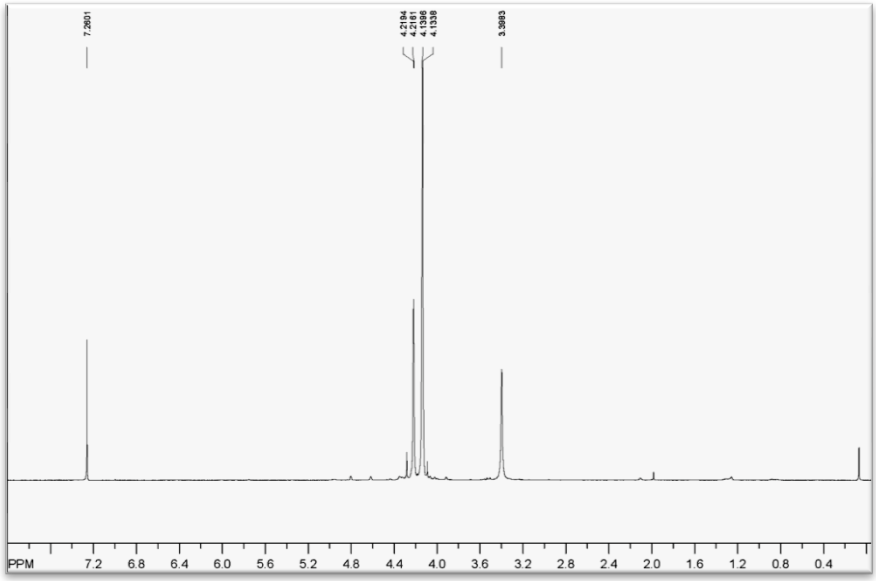

Figure 3.9 - NMR spectra of ferrocenylacetic acid, the starting compound for ferrocenylethanol synthesis.

The spectrum of purified ferrocenylethanol represented in figure 3.10 shows high similarity with previous publications for this compound (Davis et al. 2005).

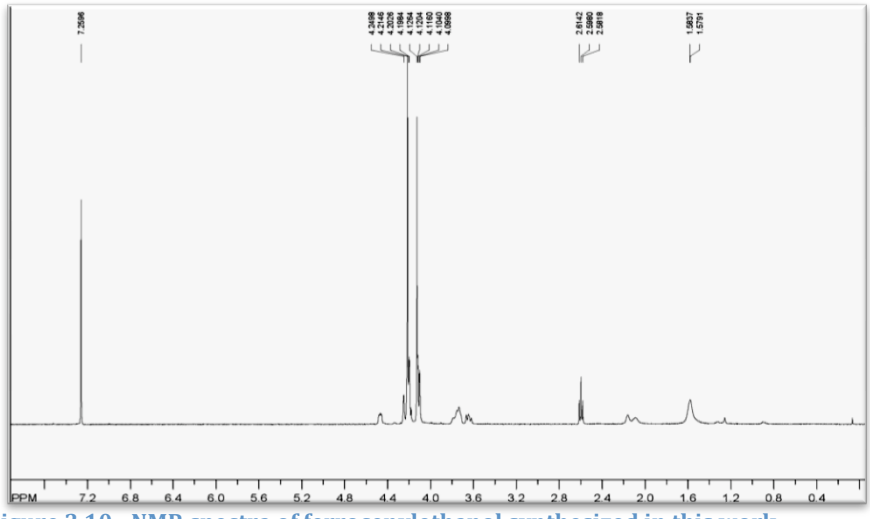

Figure 3.10 - NMR spectra of ferrocenylethanol synthesized in this work.

3.4.3 Voltammetry of mono-substituted ferrocenes

Voltammograms of each ferrocene were performed before and after the oxidation procedure. For each pH buffer solution voltammograms were acquired for the starting reduced state ferrocene and for the respective electrochemically oxidized ferrocenium. It was been shown that oxidation does not change the voltammogram. Figure 3.11 represents the voltammetric traces of ferrocenes prepared as described on section 2.4.

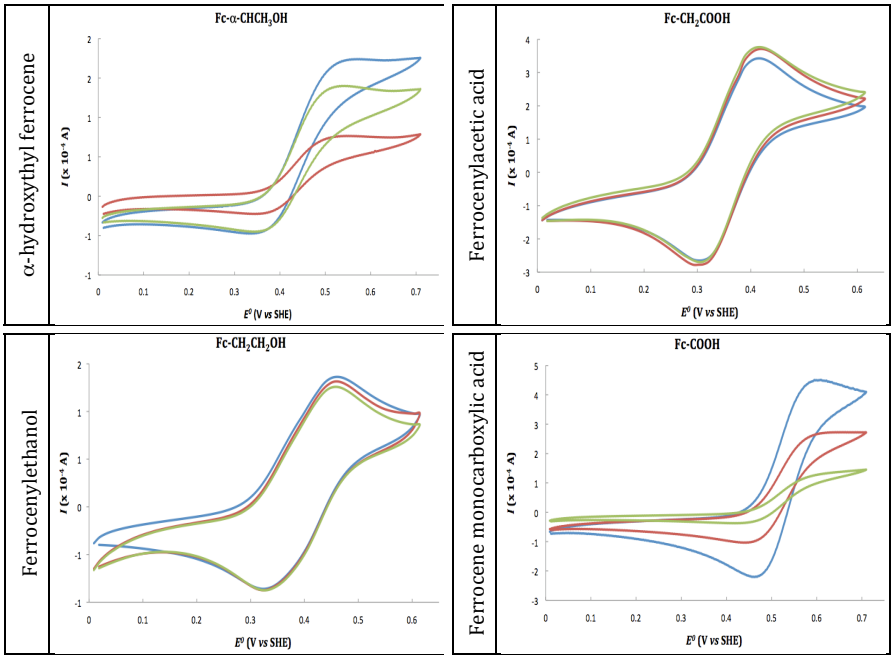

Figure 3.11 - Voltammetry of mono-substituted ferrocenes at different pH buffer solutions (pH6.0 in blue, pH 7.0 in red, pH 8.0 in green). Potentials *versus* SHE.

Table 3.2 summarizes the information of the reduction potentials for the mono-substituted ferrocenes compared with

published data (Forrow et al. 2002). The published measurements were done in acetonitrile, and herein were done in aqueous buffer solvent at different pH values. The voltammograms were analysed using SOAS software (V. Fourmond 2009) to determine the reduction potentials for each compound at different pH buffer solutions. Also, for the physiological pH range used (pH6.0 to pH8.0) the reduction potential has no appreciable modification with pH.

Comparison of reduction potentials obtained in this work with those published show high similarity even using different solvents.

3.4.1 Ferrocene oxidation

The stock solutions of mono-substituted ferrocenes prepared on section 2.4 show a yellow colour. All the mono-substituted ferrocene changes its yellow colour to blue ferrocenium, after a complete oxidation. Figure 3.12 represents the changed colour for α-hydroxyethyl ferrocene.

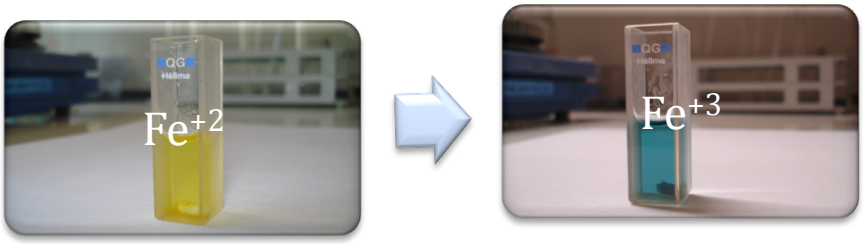

Figure 3.12 – α-hydroxyethyl ferrocene electrochemical oxidation using a potentiostat.

The obtained ferrocenia were degassed and stored for further use.

Table 3.2 – Reduction potentials of mono-substituted ferrocenes, measured in aqueous solvent, combined with previous publications. Reduction potentials *versus* SHE. Standard error was 12mV considering 10% width at half-height.

Group	Name	Structure	E^0 (mV *vs* SHE)		
			Acetonitrile solvent (Forrow *et al.* 2002)	Aqueous buffer solvent (this work)	
				pH	E^0_{red}
Alcohols	α-Hydroxyethyl ferrocene	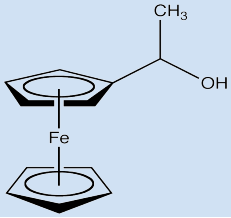	+ 416	6.0	+ 436
				7.0	+ 435
				8.0	+ 435
	Ferrocenyl ethanol	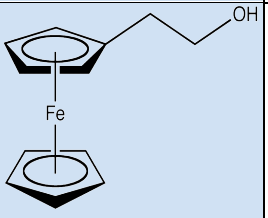	+ 361	6.0	+ 389
				7.0	+ 388
				8.0	+ 387
Carboxylic acids	Ferrocenyl acetic acid	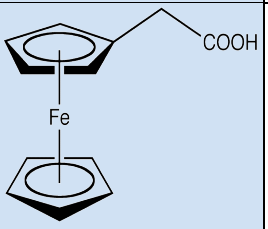	+ 361	6.0	+ 363
				7.0	+ 364
				8.0	+ 364
	Ferrocene monocarboxylic acid	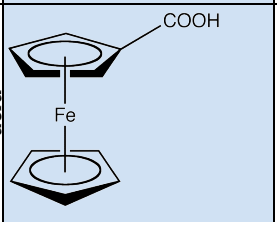	+ 516	6.0	+ 528
				7.0	+ 526
				8.0	+ 516

3.4.2 UV-Visible Spectroscopy of ferrocenes

Mono-substituted ferrocenes were studied by UV-Visible spectroscopy in the physiological pH range (pH 6.0 to pH 8.0). The reduced and oxidized spectra were compared and are

presented in figure 3.13. All mono-substituted ferrocenia presents an absorption peak maximum at 640nm. Mono-substituted ferrocenes, the reduced form, present an absorption peak maximum at 440nm.

The UV-visible spectroscopy shows that each mono-substituted ferrocene present similar spectra in the physiological pH range used (pH 6.0 to pH 8.0), both for reduced and oxidized forms. After the oxidation of mono-substituted ferrocene compounds to the respective mono-substituted ferrocenium, the lifetime of each one along overnight was studied, and reveals no significant changes.

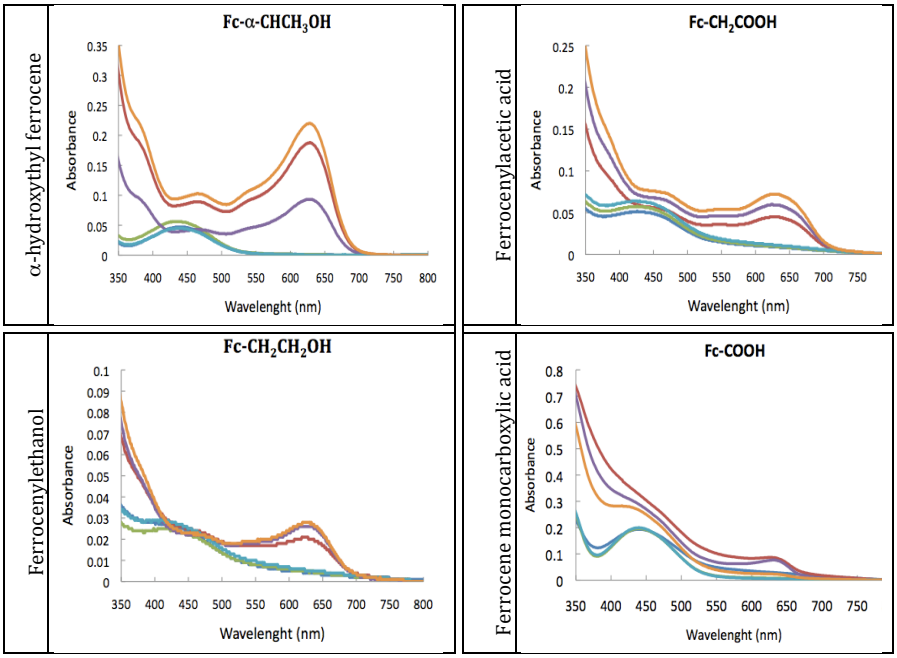

Figure 3.13 –UV-Visible spectroscopy of mono-substituted ferrocenes at different pH buffer solutions. Dark blue, pH6 red; Red, pH6 oxd; green pH7 red; purple pH7 oxd; white blue pH8 red; orange, pH8 oxd.

3.5 Cobalt complexes as mediator

3.5.1 Synthesis of *trans*-$[Co(en)_2Cl_2]^+$ and *cis*-$[Co(en)_2Cl_2]^+$

The coordination compound Dichlorobis (ethylenediamine)cobalt(III) was synthesized in both *trans* and *cis* isomer forms as described on section 2.5. Figure 3.14 represents the synthesized compounds showing a green colour for *trans*-$[Co(en)_2Cl_2]^+$ (3.14-ii) and a purple colour (3.14-iv) for *cis*-$[Co(en)_2Cl_2]^+$ complex.

Figure 3.14 – *trans* and *cis*- dichlorobis(ethylenediamine)cobalt(III) synthesis.

The synthesis was performed from reduction of 250.0mg of ferrocenylacetic acid. 10mg of Ferrocenylethanol were obtained which represents an yield of 4%.

3.5.2 Voltammetry

The complexes *trans*-$[Co(en)_2Cl_2]^+$ and *cis*-$[Co(en)_2Cl_2]^+$ were studied by voltammetry in order to analyze the reduction potentials and the purity of the synthesized compounds. Figure 3.15 presents the voltammograms of each isomer in the physiological pH range (pH6.0 to pH8.0). These results are similar to the published data in the literature (Vivier *et al.* 2006).

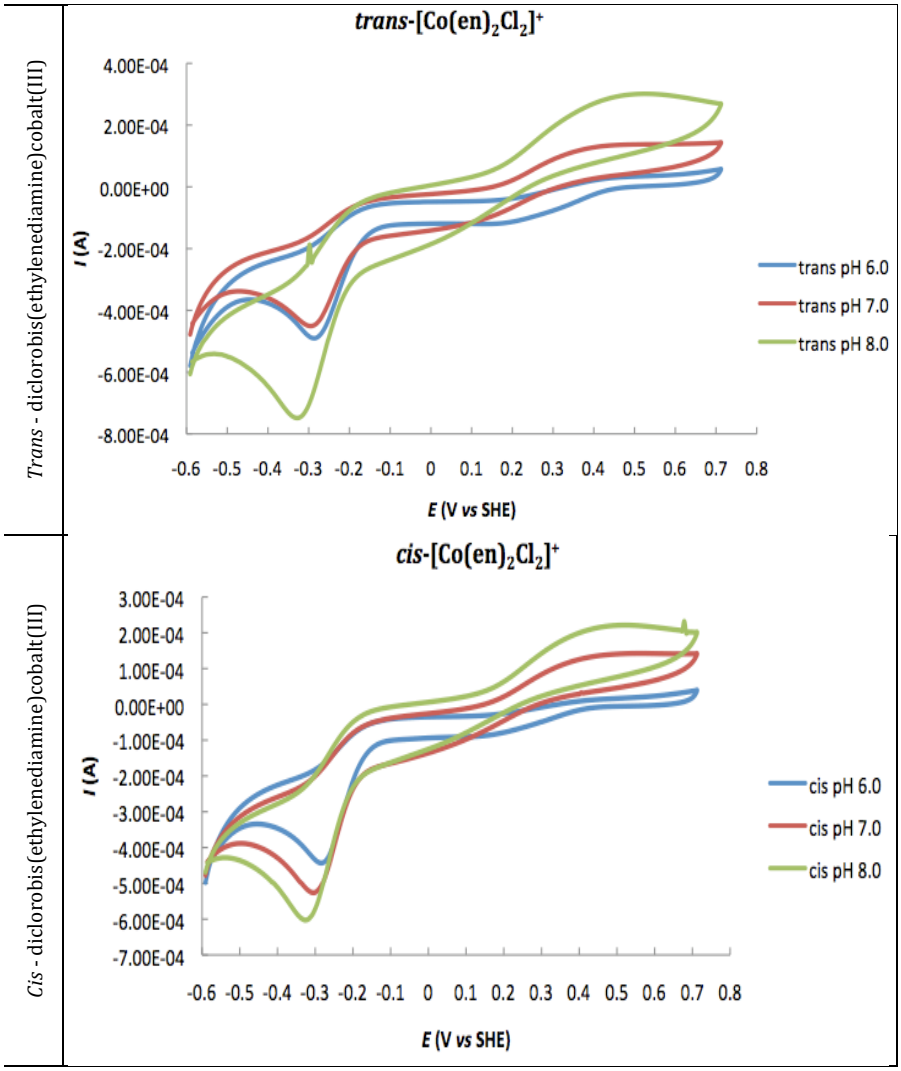

Figure 3.15 - Voltammetry of cobalt complexes at different pH buffer solutions. Potentials *versus* SHE.

The reduction potentials were determined using SOAS software (V. Fourmond 2009). The reduction potentials are presented in table 3.3.

Table 3.3 – Reduction potential of cobalt complexes at different pH buffer solutions. Standard error was 17mV considering 10% width on a half-height.

	pH	E^0 (mV)
***trans*–$[Co(en)_2Cl_2]^+$**	6.0	300
	7.0	235
	8.0	202
***cis*–$[Co(en)_2Cl_2]^+$**	6.0	266
	7.0	234
	8.0	210

The reduction potential, E^0 decreases with pH. This variation occurs for both *cis* and *trans* complex ion isomers.

3.5.3 UV-Visible Spectroscopy

To evaluate the purity of the synthesized *trans*-dichlorobis(ethylenediamine)cobalt(III) complexes, UV-visible spectroscopy were performed using different solvents (figure 3.16).

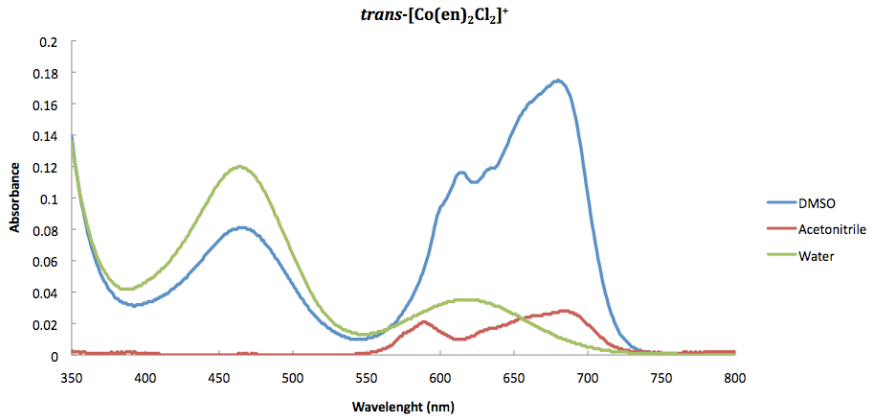

Figure 3.16 – UV-Visible spectroscopy of *trans*-dichlorobis(ethylenediamine) cobalt(III) in different solvents.

The spectra of *trans*-$[Co(en)_2Cl_2]^+$ in different protic and aprotic solvents (figure 3.16) are similar to data previously published for this compound (Vivier et al. 2006).

The stability of *trans*-$[Co(en)_2Cl_2]^+$ and *cis*-$[Co(en)_2Cl_2]^+$ in different pH buffer solutions was measured by UV-visible spectrometry. For each pH the oxidized form of *trans*-$[Co(en)_2Cl_2]^+$ was subjected to one spectroscopic scan per minute over 20 minutes. The reduction form was achieved by addition of some microlitres of sodium dithionite. The data collected is presented in figure 3.17 for each pH.

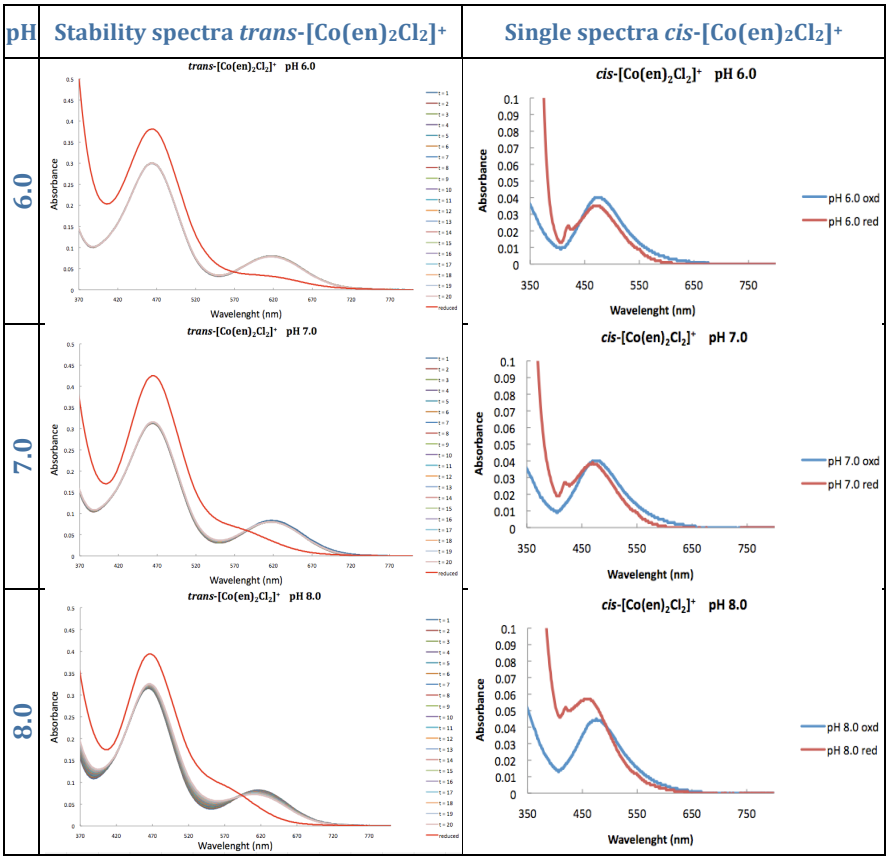

Figure 3.17 – UV-Visible spectroscopy of *trans* and *cis*-dichlorobis(ethylenediamine) cobalt(III) in different pH buffer solutions. Stability of *trans*-$[Co(en)_2Cl_2]^+$ during 20 min. Reduction with sodium dithionite.

The oxidized form of *trans*-$[Co(en)_2Cl_2]^+$ does not present a significant variation during the 20 minutes that each pH experiment lasted. Comparison between different pH solutions shows no variation in the spectra shape and peaks, pointing for the high stability of *trans*-$[Co(en)_2Cl_2]^+$. Observation of figure 3.17 shows that *trans*-$[Co(en)_2Cl_2]^+$ has two absorption peaks with max at 460nm and 620nm in the oxidized form, and after reduction the 620nm peak disappears. The obtained data are in agreement with previous publication (Vivier *et al.* 2006). The absorption peaks of *trans*-$[Co(en)_2Cl_2]^+$ has no interference with the absorption measurements at 552nm for cytochrome c_7 on the stopped-flow equipment. After one hour in aqueous solution the *trans*-$[Co(en)_2Cl_2]^+$ begins to change its green color to the similar purple color of the *cis*-$[Co(en)_2Cl_2]^+$ complex (figure 3.14).

The oxidized form of *cis*-$[Co(en)_2Cl_2]^+$ show high stability between the different pH buffer solutions, and doesn't change its colour along the time. Figure 3.17 shows an unique absorption peak max at 460nm in both oxidized and reduced forms.

3.6 Stopped-flow calibration dead time

For dead time determination on the Stopped-Flow equipment SF-61DX2 the solutions prepared in section 2.6.3 were used. Figure 3.18 presents the kinetic traces of the ascorbic acid reaction with DCPIP.

Because of the fast kinetics of the solution B_5 and B_6 (the more concentrated in ascorbic acid) these traces were not used for the dead time calculations.

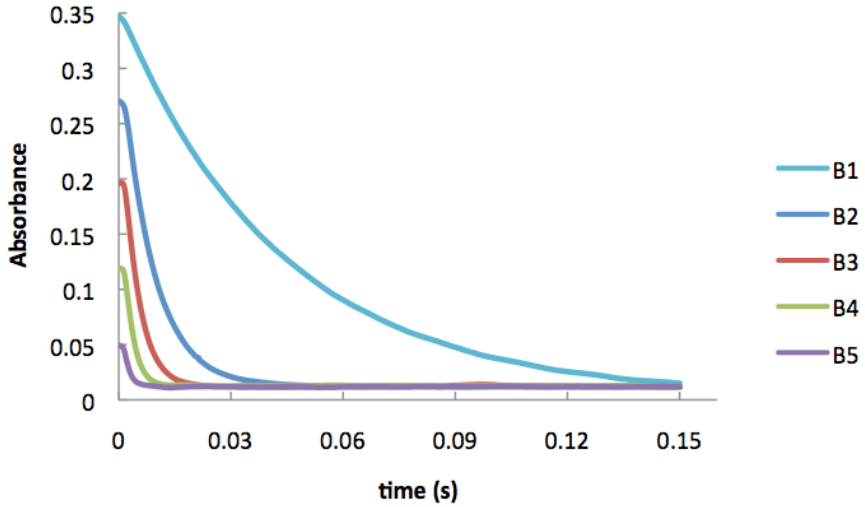

Figure 3.18 - Kinetic traces of DCPIP reaction with ascorbic acid.

The kinetic rate constants were calculated using a mono-exponential fitting, as well as the absorbance values at the beginning of the reaction. Figure 3.19 presents the data processing for dead time determination.

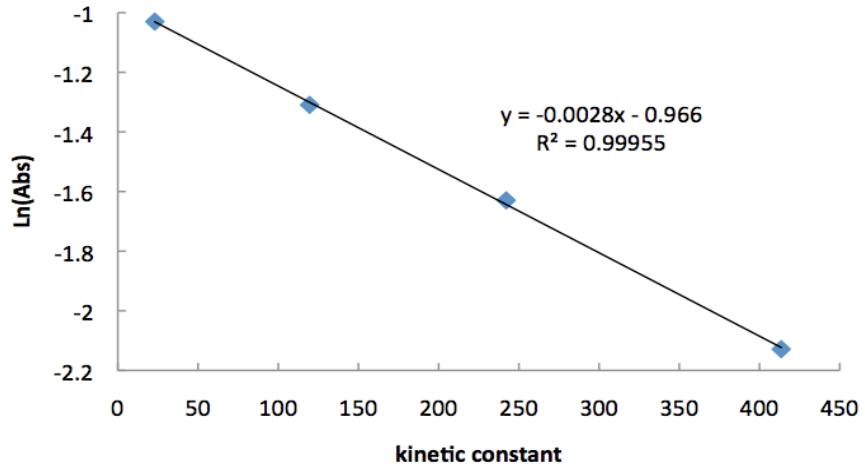

Figure 3.19 - Trend line of kinetic data from B1 to B4. The slope is the dead time.

The slope of the trend line gives a dead time of 2.8ms. Thus, the dead time used in the experiments was considered 3ms.

3.7 Kinetic experiments

The purification of cytochrome c_7 gave a few amount of protein. Because of this, the kinetic experiments with mono-substituted ferrocenes were first tested with cytochrome c_3 from *Desulfovibrio gigas*, which were not in use and it is very abounded in the lab stock.

Because *Desulfovibrio gigas* cytochrome c_3 has similar structure and thermodynamic parameters, it was assumed that the kinetic rates would also be similar to the *D. acetoxidans* cytochrome c_7. The kinetic experiment with *trans*-$[Co(en)_2Cl_2]^+$ were performed using both cytochrome c_3 (data not shown) and cytochrome c_7.

3.7.1 Kinetic data using α-hydroxyethyl ferrocenium as mediator

The α-hydroxyethyl ferrocenium was used as mediator to analyse the metal reductase activity of *Desulfovibrio gigas* cytochrome c_3. The experiments were performed using cytochrome c_3 concentration of 0.6μM in 100mM tris-maleate buffer at pH 8.0, with ionic strength set to 500mM trough addition of KCl.

Figure 3.20 illustrates the kinetic traces acquired. The blue trace shows the reaction of fully reduced cytochrome c_3

with the buffer solution. This trace works as control, for the fully reduced initial state of the cytochrome c_3.

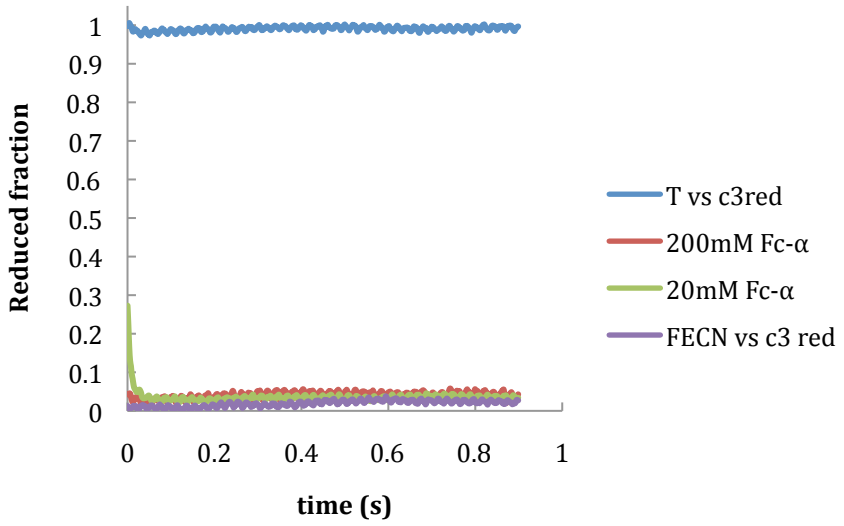

Figure 3.20 – Kinetic traces of the oxidation of *D. gigas* cytochrome c_3 by α-hydroxyethyl ferrocenium.

The red trace illustrates the reaction of α-hydroxyethyl ferrocenium, which has a 100μM concentration after mixing ensuring the pseudo first order condition. The reaction was so fast, that no kinetic curve was observed in the time scale used (0.9s). Even when the concentration of the mediator was ten times less concentrated (illustrated in green) the kinetic reaction is too fast in the time scale used (0.9s). The after mixing concentration was 10μM abolishing the pseudo first order condition. To certify that the cytochrome c_3 was fully oxidized, an experiment with excess of potassium ferricyanide was performed, corresponding to the fully oxidized state of the cytochrome c_3.

After each experiment, UV-visible spectra were obtained in order to follow the redox process (figure 3.21). The shift in the *Soret* band and the broadening of the α and β bands allows to follow the fully reduced and fully oxidized states of the cytochrome c_3.

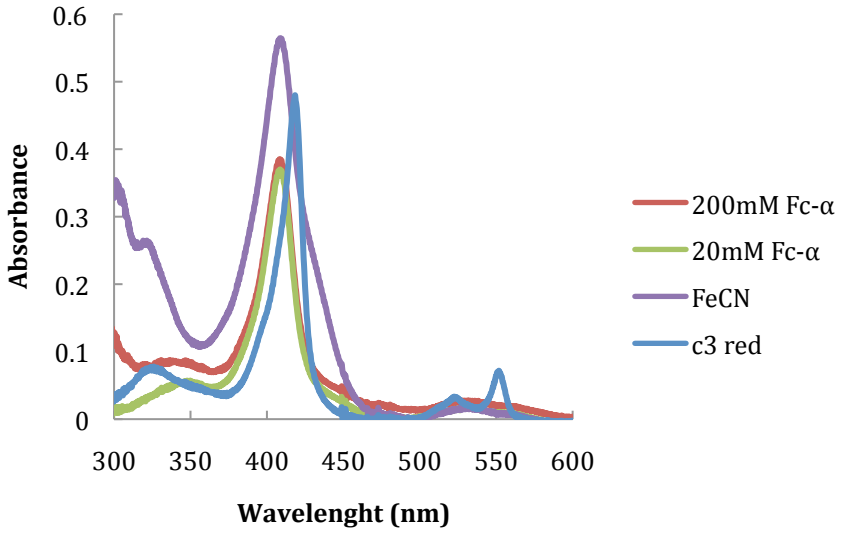

Figure 3.21 – UV-visible spectroscopy of cytochrome c_3 along the kinetic experiments.

3.7.2 Kinetic data using *trans*-$[Co(en)_2Cl_2]^+$ as mediator

The kinetic data obtained for the oxidation of triheme cytochrome c_7 by *trans*-$[Co(en)_2Cl_2]^+$ at different pH values (7.04 and 8.08) and the fitted curves using the kinetic model described in the materials and methods section are presented in figure 3.22.

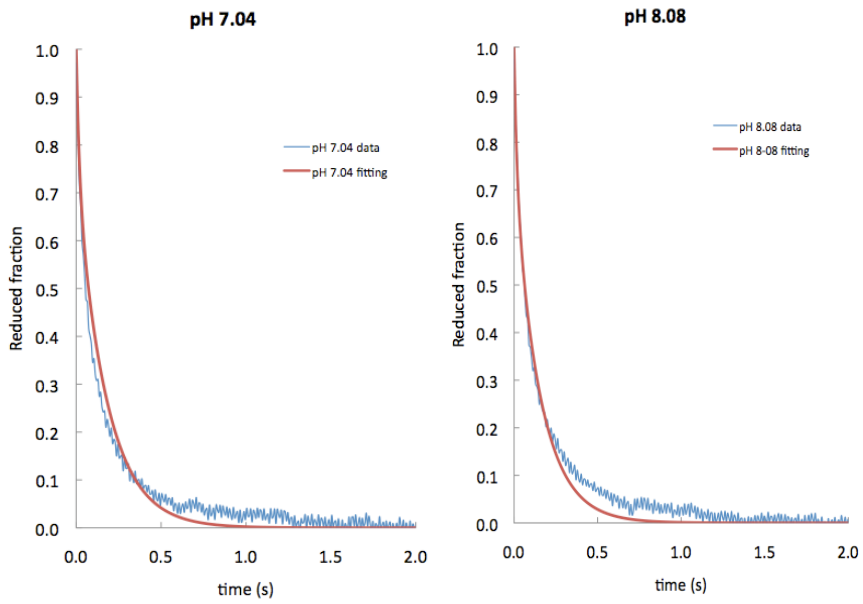

Figure 3.22 - Kinetics of oxidation of cytochrome c_7 by *trans*-$[Co(en)_2Cl_2]^+$ at pH 7.04 and 8.08. The blue continuous lines are the fit of the data using the thermodynamic parameters.

The rate constants, k_i^0 obtained are presented in table 3.4.

Table 3.4 – Reference rate constants for each heme of *D. acetoxidans* cytochrome c_7. Standard errors of the kinetic traces are given in *parenthesis*.

Reference rate constants k_i^0 ($x\ 10^3\ M^{-1}s^{-1}$)	**Heme I**	**Heme III**	**Heme IV**
Cytochrome c_7	31.7 (5.2)	3.3 (7.2)	0.0 (5.1)

4 Discussion

4.1 Mono-substituted ferrocenium as mediator

The α-hydroxyethyl ferrocenium was used as mediator to analyse the metal reductase activity of *D. gigas* cytochrome c_3 at pH 8.0. The cytochrome c_3 concentration was 0.6μM and the α-hydroxyethyl ferrocenium concentration was 100μM. The large excess of reducing agent relative to the concentration of the protein was set to guarantee irreversible electron transfer steps and pseudo first order conditions. The reaction between α-hydroxyethyl ferrocenium and cytochrome c_3 is complete in the lead-time of the stopped-flow. In fact, the large difference between the reduction potentials of the electron donor (cytochrome c_3) and the electron acceptor (α-hydroxyethyl ferrocenium) is large enough to set an huge ΔG^0 that, according to Marcus equation (Marcus & Sutin 1985) enhances the electron transfer rate, k_{ET}, making it too fast to follow by stopped-flow methods.

The mono-substituted ferrocenes prepared on this work, have very positive reduction potentials (table 3.1). The tested α-hydroxyethyl ferrocenium has a potential of 435mV, which corresponds to an intermediate value when compared with the others. The advantage for the use of mono-substituted ferrocenes were the comparison on the electron transfer rates using similar structures with different reduction potential,

which generate different driving forces. The tested mono-substituted ferrocene shows too fast electron transfer reaction, which indicates that other mono—substituted ferrocenes with highest reduction potential (and obviously larger driving force) will not give any information. Furthermore, even if any other mono-substituted ferrocene with lower reduction potential (meaning lower driving forces) could give measurable information, could not be compared to the desire parameters.

For this reason, the mono-substituted ferrocenia prepared in this work cannot be applied to measure the kinetic of oxidation of the cytochrome c_7, using the stopped-flow technique.

4.2 Cobalt complexes as mediators

The synthesized cobalt complexes *trans*-$[Co(en)_2Cl_2]^+$ and *cis*-$[Co(en)_2Cl_2]^+$ show different characteristics in their absorption spectra. It was possible to compare the absorption spectra of *trans*-$[Co(en)_2Cl_2]^+$ with the previous publications and ensure the successful synthesis. On the other hand, no data were found in the literature for the analysis and comparison of the *cis*-$[Co(en)_2Cl_2]^+$ spectra. Studies of *trans*-$[Co(en)_2Cl_2]^+$ in aqueous solution shows that aquation reaction occurs by the substitution of one Cl^- by a water molecule (Moura *et al.* 2006). This reaction was followed by the change in colour from green to purple where the kinetic depends on the temperature. The synthesized *cis*-$[Co(en)_2Cl_2]^+$ complex presents the purple

colour described, but some questions remain unclear. Given the lack of spectroscopic standards in the literature, the possibility of having two species in solution cannot be discarded.

That way, the use of *cis*-$[Co(en)_2Cl_2]^+$ as mediator for the oxidation study of cytochrome c_7 was excluded. The certification of purity and stability of *trans*-$[Co(en)_2Cl_2]^+$ makes it a convenient choice for the present work.

The kinetic model is applicable to systems such as that used in this work, in which there is fast intramolecular and slow intermolecular electron exchange on the stopped-flow time scale. Application of the model depends also on the existence of a detailed thermodynamic characterisation of the multicenter redox protein (Catarino & Turner 2001), as the case for the cytochromes c_3 and c_7.

The known thermodynamic characterisation of cytochrome c_7 (Correia et al. 2002) and the excess of oxidant agent (*trans*-$[Co(en)_2Cl_2]^+$) relative to the concentration of the protein guarantee the requisites for application of kinetic model (Catarino & Turner 2001). The present modelling shows to be an useful tool to acquire information about the microscopic redox steps from the measurable macroscopic rate constants.

Table 4.1 collects all the thermodynamic parameters of cytochrome c_7 from *D. acetoxidans* reported in the literature (Correia *et al.* 2002).

Table 4.1 – Thermodynamic parameters of cytochrome c_7 from *D. acetoxidans* (Correia *et al.* 2002).

	Heme I	Heme III	Heme IV	Ionisable Centre
Heme I	**-201** (4)	19 (2)	3 (2)	2 (4)
Heme III		**-200** (3)	26 (2)	14 (3)
Heme IV			**-142** (4)	-5 (4)
Ionisable Centre				**486** (10)

Three rate constants, k_i^0 (table 3.3) intrinsic to each heme of cytochrome c_7 were fit to the kinetic data illustrated in figure 3.22 of the results section.

The single electron transfer reduction of cobalt (III) to cobalt (II) by cytochrome c_7 shows that the k_i^0 of heme I has the highest value, while heme IV has a negligible k_i^0. Looking for the thermodynamic parameters of cytochrome c_7 (table 4.1), is possible to see that heme IV would compete lower driving force when compared with heme I and heme III.

Because heme IV has the more positive reduction potential, the difference between this center and the metal complex reduction potential will be lower when compared with the other hemes. According to the Marcus theory (Marcus & Sutin 1985), lower driving forces lead to lower kinetic rate constants for single electron transfer. This evidence is in agreement with the fact that the reference rate constant of heme IV is negligible when compared with the other hemes. Comparison with previous work (Correia *et al.* 2002) it is possible to observe that

the driving force is not the sole factor that controls the rates. When reducing with sodium dithionite the greater driving force is with heme IV and when oxidizing with *trans*-$[Co(en)_2Cl_2]^+$ the greater driving force is with heme I. However in both cases the interaction occurs between the redox mediator and heme I.

The surface exposure of each heme to the solution, also influences the interaction between the hemes and the metal complex. The calculation of the solvent exposure was made, based on the weighted average surface accessibility for water. Considering a radius of 1.4Å for water molecule (Zhang & Xu 1995) the weighted average of relative accessibilities were 237:215:177 for heme I, IV and III respectively. The large exposure of heme I facilitates the interaction of the metal complex with the cytochrome, and therefore is in agreement with the largest rate constant for this heme.

Furthermore, the electrostatic environment of the protein is another characteristic that influences the interaction with redox partners. Figure 4.1 represents the electrostatic environment as a result of the charges of the amino acid residues in the polypeptide chain of cytochrome c_7.

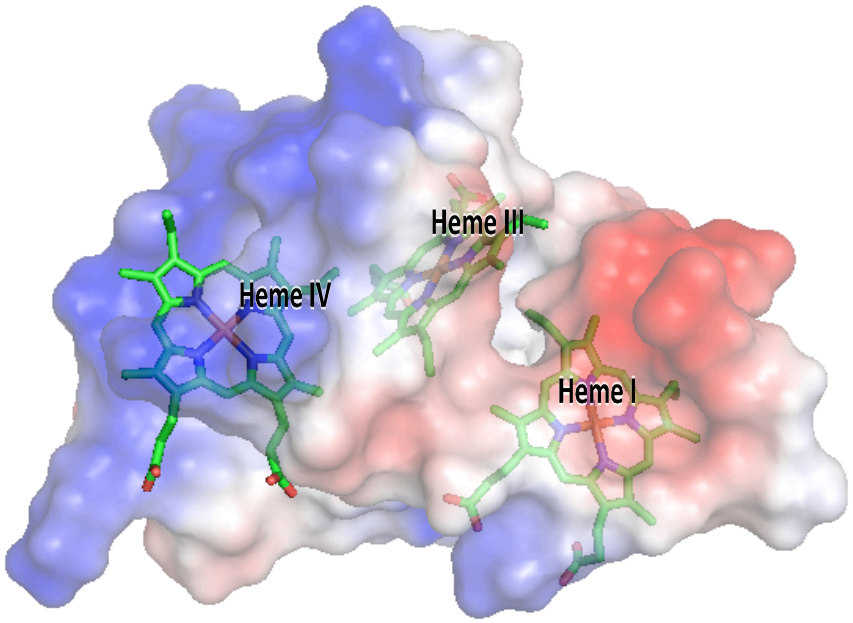

Figure 4.1 – Electrostatic environment around the hemes of fully reduced cytochrome c_7 from *D. acetoxidans* adapted from the structure data assigned by NMR (Assfalg et al. 1999).

In the electrostatic surface of cytochrome c_7 it is possible to distinguish the negative electrostatic density (in red) near heme I, and the positive electrostatic density (in blue) around heme IV.

Since the positive charge of *trans*-$[Co(en)_2Cl_2]^+$ favours the interaction with negative residues of the protein, the electrostatic charges of cytochrome c_7 are in agreement with the observation that heme I is the fastest electron donor. This heme is surrounded by an aspartate, a glutamate and propionate acidic residues (Czjzek et al. 2001) which makes the environment around the heme I negative, promoting the interaction with the cobalt complex.

On the other hand, previous work on reduction of chromium (VI) to chromium (III) by cytochrome c_7 has shown that the site of interaction between chromium (III) and cytochrome c_7 is close to heme IV (Assfalg et al. 2002). This difference may result from the fact that heme IV is surrounded by positive surface charges, known as lysine patch (Louro 2007). The specific binding site verified in Assfalg work (Assfalg et al. 2002) is created by the interaction of the negative charge from CrO_4^{2-} with the positive charge in the vicinity of heme IV due to the presence of four lysine residues.

These results show that the less exposed heme III appears to play a minor role in the intermolecular electron transfer processes of cytochrome c_7.

To determine the relative importance of each heme in the oxidation process of *Desulfuromonas acetoxidans* was compared. The fraction of electrons that leaves the molecule through each heme in each oxidation step was calculated from the product of the reference rate constants and the population distribution given by the thermodynamics (the microscopic rate constants, k_i). Table 4.2 collect these values from the oxidation process with *trans*-$[Co(en)_2Cl_2]^+$ and compares with the previous obtained data from the reduction with dithionite (Correia *et al.* 2002). The values of the oxidation process show that heme I work as the main exit gate, and only a small percentage of oxidation occurs through heme III.

Table 4.2 – Fraction of electrons that enter and leave the molecule through each heme in each one-electron reduction step. Comparison the published data for reduction with dithionite (Correia *et al.* 2002) with the data for oxidation with *trans*-$[Co(en)_2Cl_2]^+$.

	Reduction with dithionite			Oxidation with *trans*-$[Co(en)_2Cl_2]^+$		
Step	**Heme I**	**Heme III**	**Heme IV**	**Heme I**	**Heme III**	**Heme IV**
1	0.82	0	0.18	0.96	0.04	0
2	0.96	0	0.04	0.74	0.26	0
3	0.98	0	0.02	0.80	0.20	0

Comparison with previous work (table 4.2) of the reduction of cytochrome c_7 (Correia et al. 2002) shows that the electrons enter the cytochrome mainly via heme I, the more exposed heme. In both cases of reduction and oxidation of the cytochrome c_7 heme I plays the key role for the electron transfer processes. In the case of the oxidation process, is possible to conclude that there are several reasons for that, like the electrostatic charge of protein around heme I, the surface exposure of the hemes and the driving force between the hemes and the metal complex.

5 Conclusion

Recently, substantial advances have been made to understand the biochemical processes that control the electron transfer reactions of metalloproteins. The development of methods for the detailed analysis of complex reaction mechanisms provides an important drive towards to this end (Catarino & Turner 2001, Fonseca *et al.* 2009, Pessanha *et al.* 2009).

Comparison of the oxidation of cytochrome c_7 by cobalt complex reported in this work with the literature shows that complementarities between the contact surfaces of donor and acceptor (Louro *et al.* 2001b, Louro *et al.* 2004) appear to be the major contributor towards the molecular mechanism for the electron transfer. This does not mean, as reported for the reduction of cytochrome c_7 with dithionite that other factors such as surface exposure cannot give a significant contribution (Correia *et al.* 2002).

The routines implemented in present work, may be used for other cytochromes (like cytochrome c_3 from *Desulfovibrio gigas* also tested in this work) in order to understand the unknown oxidation mechanisms of these proteins. That way in the near future it will be possible to correlate the molecular redox mechanisms from different organisms, and better understand the relationship between the structure and function of proteins.

The selection of redox partners with the strictly required

characteristic features remains a difficult challenge. Future goals will be the application of different metal complexes with properties like: similar reduction potentials and size but different charges; similar reduction potentials and charges but different sizes; equal charges and similar size but different reduction potentials. The application of ferrocenes with lower reduction potentials as mediators will provide these features to determine the most important parameter in the interaction of redox centers. Design and synthesis of new compounds with such features will provide new tools as redox mediators in biorganometallic chemistry.

Application of different techniques like flash photolysis that allows the measurement of fast kinetic reactions on shorter time scales (sub-microsecond time scale), will increase the range of redox partners that could be used. That way will be possible to follow fast electron transfer rates from higher driving force redox centers. Another promising method is a newly continuous-flow mixing device, which has a perfect mixing efficiency with a higher time resolution close to 160μs (Akiyama *et al.* 2002). Combined use of the developed device with spectrometric system will enable the access of information for the electron transfer of proteins in solution in the microsecond time domain.

Design new mutants of cytochromes to study the interaction site with known redox partners and new ones. For example, application of site-directed mutagenesis in cytochrome c_7 to prepare a modified cytochrome where the

glutamic acid and the aspartic acid residues near heme I are substituted by neutral charged nonpolar residues like alanine. This proposal would clarify the relevance of the electrostatic charges of the amino acids in the surrounding area of the hemes, and its control on the interaction site for electron transfer reactions.

Understand the mechanism of electron transfer of cytochromes with few hemes is the starting point for further studies with cytochromes with more heme groups, like the nine-heme cytochrome c from *Desulfovibrio desulfuricans*, or the sixteen-heme cytochrome c from *Desulfovibrio gigas* and *Desulfovibrio vulgaris*. The draft genome of *Desulfuromonas acetoxidans* shows that there are 33 putative *c*-type cytochromes in this organism with up to 12 hemes per polypeptide chain. The importance of the large number of hemes in multiheme cytochromes, and its relevance for the metabolic pathways of microorganisms remains unclear. However, they have been shown to play a key role in metal reduction metabolic pathways of their host organisms and therefore a better understanding of their function bears implications for biogeochemistry as well as bioremediation of contaminated environments and assembly of microbial fuel cells.

6 Bibliography

Akiyama, S., Takahashi, S., Kimura, T., Ishimori, K., Morishima, I., Nishikawa, Y., and Fujisawa, T. (2002) "Conformational landscape of cytochrome c folding studied by microsecond-resolved small-angle x-ray scattering". *Proc. Natl. Acad. Sci.* **99**, 1329-1334.

Ambler, R. P. (1991) "Sequence variability in bacterial cytochromes c". *Biochim. Biophys. Acta* **1058**, 42-47.

Assfalg, M., Banci, L., Bertini, I., Bruschi, M., Giudici-Orticoni, M. T., and Turano, P. (1999) "A proton-NMR investigation of the fully reduced cytochrome c_7 from *Desulfuromonas acetoxidans*. Comparison between the reduced and the oxidized forms". *Eur. J. Biochem.* **266**, 634-643.

Assfalg, M., Bertini, I., Bruschi, M., Michel, C., and Turano, P. (2002) "The metal reductase activity of some multiheme cytochromes *c*: NMR structural characterization of the reduction of chromium(VI) to chromium(III) by cytochrome c_7". *Proc. Nat. Acad. Sci.* **99**, 9750-9754.

Bailar, J. (1946) "Cis-and trans-dichlorobis (ethylenediamine) cobalt (III) chloride and the resolution of the *cis* form". *Inorg. Synth* **2**, 223.

Bailar, J. C. (1936) "The Stereochemistry of Complex Inorganic Compounds". *Chem. Rev.* **19**, 67-87.

Bailar, J. (1953) "*Inorganic syntheses"*, McGraw-Hill, New York.

Brown, G. E., Jr., Henrich, V. E., Casey, W. H., Clark, D. L., Eggleston, C., Felmy, A., Goodman, D. W., Gratzel, M., Maciel, G., McCarthy, M. I., Nealson, K. H., Sverjensky, D. A., Toney, M. F., and Zachara, J. M. (1999) "Metal Oxide

Surfaces and Their Interactions with Aqueous Solutions and Microbial Organisms". *Chem. Rev.* **99**, 77-174.

Capeillere-Blandin, C., Barber, M. J., and Bray, R. C. (1986) "Comparison of the processes involved in reduction by the substrate for two homologous flavocytochromes b2 from different species of yeast". *Biochem. J.* **238**, 745-756.

Catarino, T. (1998) "Thermodynamic and kinetic modelling of the redox properties of tetrahaem cytochromes c_3". PhD Thesis, Universidade Nova de Lisboa, Lisbon.

Catarino, T., and Turner, D. L. (2001) "Thermodynamic control of electron transfer rates in multicentre redox proteins". *Chembiochem.* **2**, 416-424.

Christensen, H. E. M., Coutinho, I., Conrad, L. S., Hammerstadpedersen, J. M., Iversen, G., Jensen, M. H., Karlsson, J. J., Ulstrup, J., and Xavier, A. V. (1994) "Electron-Transport Networks in Multicenter Metalloproteins". *J. Photochem. Photobiol., A* **82**, 103-115.

Cornell, R., and Schwertmann, U. (2003) "*The iron oxides: Structure, properties, reactions, occurrences, and uses"*, Wiley-VCH, Weinheim.

Correia, I. J., Paquete, C. M., Louro, R. O., Catarino, T., Turner, D. L., and Xavier, A. V. (2002) "Thermodynamic and kinetic characterization of trihaem cytochrome c_3 from *Desulfuromonas acetoxidans*". *Eur. J. Biochem.* **269**, 5722-5730.

Czjzek, M., Arnoux, P., Haser, R., and Shepard, W. (2001) "Structure of cytochrome c_7 from *Desulfuromonas acetoxidans* at 1.9 A resolution". *Acta Crystallogr., Sect D: Biol. Crystallogr.* **57**, 670-678.

Davis, W. L., Shago, R. F., Langner, E. H. G., and Swarts, J. C. (2005) "Synthesis and electrochemical properties of a

series of ferrocene-containing alcohols". *Polyhedron* **24**, 1611-1616.

De Francesco, R., Edmondson, D. E., Moura, I., Moura, J. J., and LeGall, J. (1994) "Kinetic studies on the electron-transfer reaction between cytochrome c_3 and flavodoxin from *Desulfovibrio vulgaris* strain Hildenborough". *Biochemistry* **33**, 10386-10392.

Dixon, M. (1971) "The acceptor specificity of flavins and flavoproteins. I. Techniques for anaerobic spectrophotometry". *Biochim. Biophys. Acta* **226**, 241-258.

Fonseca, B. M. (2007) "Preliminary studies of terminal reductases from the respiratory chains of *Desulfuromonas acetoxidans*". MSc Thesis, Universidade Nova de Lisboa, Lisbon.

Fonseca, B. M., Saraiva, I. H., Paquete, C. M., Soares, C. M., Pacheco, I., Salgueiro, C. A., and Louro, R. O. (2009) "The tetraheme cytochrome from *Shewanella oneidensis* MR-1 shows thermodynamic bias for functional specificity of the hemes". *J. Biol. Inorg. Chem.* **14**, 375-385.

Forrow, N., Sanghera, G., and Walters, S. (2002) "The influence of structure in the reaction of electrochemically generated ferrocenium derivatives with reduced glucose oxidase". *J. Chem. Soc., Dalton Trans.* **2002**, 3187-3194.

Fredrickson, J. K., and Gorby, Y. A. (1996) "Environmental processes mediated by iron-reducing bacteria". *Curr. Opin. Biotechnol.* **7**, 287-294.

Gebhardt, N. A., Thauer, R. K., Linder, D., Kaulfers, P. M., and Pfennig, N. (1985) "Mechanism of Acetate Oxidation to Co-2 with Elemental Sulfur in *Desulfuromonas acetoxidans*". *Arch. Microbiol.* **141**, 392-398.

Giudici-Orticoni, M. T., Makarov, A. A., Lobachov, V. M., Protasevich, I. I., Lexa, D., and Bruschi, M. (2003) "Conformational properties of multihemic cytochromes *c* from *Desulfuromonas acetoxidans*". *Thermochim. Acta* **397**, 5-12.

Haworth, D. T., Neuzil, E. F., and Kittsley, S. L. (1955) "On the Rate of the cis-trans Interconversion of Dichlorobis-(ethylenediamine)-cobalt(III) Chloride". *J. Am. Ceram. Soc.* **77**, 6198-6198.

Hungate, R. E. (1969) "A Roll Tube Method for Cultivation of Strict Anaerobes ". *Methods Microbiol.* **3B**, 117-132.

Ives, D., Janz, G., and King, C. (1961) "Reference electrodes: theory and practice". *J. Electrochem. Soc.* **108**, 246C.

Lagarias, J., Reeds, J., Wright, M., and Wright, P. (1998) "Convergence properties of the Nelder-Mead simplex algorithm in low dimensions". *SIAM J. Optim.* **9**, 112-147.

Levitt, M. (2001) "*Spin dynamics: basics of nuclear magnetic resonance"*, Wiley, New York.

Louro, R. O., Catarino, T., LeGall, J., and Xavier, A. V. (1997) "Redox-Bohr effect in electron/proton energy transduction: cytochrome c_3 coupled to hydrogenase works as a 'proton thruster' in *Desulfovibrio vulgaris*". *Journal of Biological Inorganic Chemistry* **2**, 488-491.

Long, N. (1998) "*Metallocenes: an introduction to sandwich complexes"*, Blackwell Science, Oxford.

Louro, R. O., Catarino, T., LeGall, J., Turner, D. L., and Xavier, A. V. (2001b) "Cooperativity between electrons and protons in a monomeric cytochrome c_3: the importance of mechano-chemical coupling for energy transduction". *Chembiochem.* **2**, 831-837.

Louro, R. O., Catarino, T., Paquete, C. M., and Turner, D. L. (2004) "Distance dependence of interactions between charged centres in proteins with common structural features". *FEBS Lett.* **576**, 77-80.

Louro, R. O. (2007) "Proton thrusters: overview of the structural and functional features of soluble tetrahaem cytochromes c_3". *J. Biol. Inorg. Chem.* **12**, 1-10.

Lovley, D. R., and Phillips, E. J. (1988) "Novel Mode of Microbial Energy Metabolism: Organic Carbon Oxidation Coupled to Dissimilatory Reduction of Iron or Manganese". *Appl. Environ. Microbiol.* **54**, 1472-1480.

Lovley, D. R., Baedecker, M. J., Lonergan, D. J., Cozzarelli, I. M., Phillips, E. J. P., and Siegel, D. I. (1989) "Oxidation of Aromatic Contaminants Coupled to Microbial Iron Reduction". *Nature* **339**, 297-300.

Lovley, D. R. (1991) "Dissimilatory Fe(Iii) and Mn(Iv) Reduction". *Microbiol. Rev.* **55**, 259-287.

Lovley, D. R. (1993) "Dissimilatory metal reduction". *Annu. Rev. Microbiol.* **47**, 263-290.

Lovley, D. R., and Coates, J. D. (1997) "Bioremediation of metal contamination". *Curr. Opin. Biotechnol.* **8**, 285-289.

Marcus, R. A. (1956) "Theory of Oxidation-Reduction Reactions Involving Electron Transfer .1.". *J. Chem. Phys.* **24**, 966-978.

Marcus, R., and Sutin, N. (1985) "Electron transfers in chemistry and biology". *Biochim. Biophys. Acta* **811**, 265-322.

Matsumura, K., Enoki, Y., Kohzuki, H., and Sakata, S. (1990) "A simple procedure for determination of the dead time of a stopped-flow instrument". *Jpn. J. Physiol.* **40**, 567-571.

Miller, T. L., and Wolin, M. J. (1974) A serum bottle modification of the Hungate technique for cultivating obligate anaerobes. Am. Soc. Microbiol.

Moore, G., and Pettigrew, G. (1990) "*Cytochromes c: evolutionary, structural and physicochemical aspects"*, Springer-Verlag, Berlin.

Moura, A., Martins, P., Cunha, L., Bolzon, L., Pertusatti, J., and Prado, A. (2006) "Estudos cinéticos da aquação do [trans-$Co(en)_2Cl_2$]Cl". *Quim. Nova* **29**, 385-387.

Moura, J. G., Moore, G. R., Williams, R. J., Probst, I., Legall, J., and Xavier, A. V. (1984) "Nuclear-magnetic-resonance studies of *Desulfuromonas acetoxidans* cytochrome c551.5 (c7)". *Eur. J. Biochem.* **144**, 433-440.

Nealson, K. H. (1997) "Sediment bacteria: who's there, what are they doing, and what's new?". *Annu. Rev. Earth Planet Sci.* **25**, 403-434.

Nealson, K. H., and Saffarini, D. (1994) "Iron and manganese in anaerobic respiration: environmental significance, physiology, and regulation". *Annu. Rev. Microbiol.* **48**, 311-343.

Niederhoffer, E. C., Peascoe, R., Rudolf, P. R., Clearfield, A., and Martell, A. E. (1986) "Structure of trans-dichlorobis(ethylenediamine)cobalt(III) perchlorate". *Acta Crystallographica Section C* **42**, 568-570.

Paquete, C. M. (2006) "Thermodynamic and kinetic characterisation of multiheme cytochromes". PhD Thesis, Universidade Nova de Lisboa, Lisbon.

Paquete, C., Turner, D., Louro, R., Xavier, A., and Catarino, T. (2007) "Thermodynamic and kinetic characterisation of individual haems in multicentre cytochromes c3". *Biochim. Biophys. Acta, Bioenerg.* **1767**, 1169-1179.

Pearson, R. G., and Basolo, F. (1956) "Mechanism of Substitution Reactions of Complex Ions. X. ii-Bonding in Dissociation Reactions of Octahedral Complexes1,2". *Journal of the American Chemical Society* **78**, 4878-4883.

Pereira, I. A., Pacheco, I., Liu, M. Y., Legall, J., Xavier, A. V., and Teixeira, M. (1997) "Multiheme cytochromes from the sulfur-reducing bacterium *Desulfuromonas acetoxidans*". *Eur J Biochem* **248**, 323-328.

Pessanha, M., Rothery, E. L., Miles, C. S., Reid, G. A., Chapman, S. K., Louro, R. O., Turner, D. L., Salgueiro, C. A., and Xavier, A. V. (2009) "Tuning of functional heme reduction potentials in *Shewanella* fumarate reductases". *Biochim. Biophys. Acta* **1787**, 113-120.

Pfennig, N., and Biebl, H. (1976) "*Desulfuromonas acetoxidans* gen. nov. and sp. nov., a new anaerobic, sulfur-reducing, acetate-oxidizing bacterium". *Arch. Microbiol.* **110**, 3-12.

Probst, I., Bruschi, M., Pfennig, N., and Le Gall, J. (1977) "Cytochrome c-551.5 (c7) from *Desulfuromonas acetoxidans*". *Biochim. Biophys. Acta* **460**, 58-64.

Rache, R., Kroneck, P., Merkle, H., and Beinert, H. (1983) "A survey of EPR-detectable components in sulfur-reducing bacteria". *Biochim. Biophys. Acta, Protein Struct. Mol. Enzymol.* **722**, 417-426.

Rinehart Jr, K., Curby Jr, R., and Sokol, P. (1957) "Organic Chemistry of Ferrocene. II. The Preparation of Ferrocenyl Aliphatic". *J. Am. Chem. Soc* **79**, 3420-3424.

Roden, E. E., and Lovley, D. R. (1993) "Dissimilatory Fe(III) Reduction by the Marine Microorganism *Desulfuromonas acetoxidans*". *Appl. Environ. Microbiol.* **59**, 734-742.

Silva, M., Pombeiro, A., Fraústo da Silva, J., Herrmann, R., Deus, N., and Bozak, R. (1994) "Redox potential and

substituent effects in ferrocene derivatives. II". *J. Organomet. Chem.* **480**, 81-90.

Simonneaux, G., and Bondon, A. (2005) "Mechanism of electron transfer in heme proteins and models: the NMR approach". *Chem Rev* **105**, 2627-2646.

Stepnicka, P. (2008) "*Ferrocenes: Ligands, Materials and Biomolecules"*, Wiley, Prague.

Togni, A., Hayashi, T., and InterScience, W. (1995) "*Ferrocenes: homogeneous catalysis, organic synthesis, materials science"*, VCH Weinheim, Weinheim.

V. Fourmond, K. H., H. A. Heering, C. Baffert, F. Leroux, P. Bertrand, C. Léger. (2009) "SOAS: a free software to analyse electrochemical data and other one-dimensional signals". *Bioelectrochemistry*, in press

van Staveren, D. R., and Metzler-Nolte, N. (2004) "Bioorganometallic chemistry of ferrocene". *Chem. Rev.* **104**, 5931-5985.

Vargas, M., Kashefi, K., Blunt-Harris, E. L., and Lovley, D. R. (1998) "Microbiological evidence for Fe(III) reduction on early Earth". *Nature* **395**, 65-67.

Vivier, V., Aguey, F., Fournier, J., Lambert, J.-F., Bedioui, F., and Che, M. (2006) "Spectroscopic and Electrochemical Study of the Adsorption of $[Co(en)_2Cl_2]Cl$ on y-Alumina: Influence of the Alumina Ligand on Co(III)/(II) Redox Potential". *J. Phys. Chem. B* **110**, 900-906.

Weber, K. A., Achenbach, L. A., and Coates, J. D. (2006) "Microorganisms pumping iron: anaerobic microbial iron oxidation and reduction". *Nat. Rev. Microbiol.* **4**, 752-764.

Wuthrich, K. (1986) "*NMR of proteins and nucleic acids"*, Wiley, Michigan.

Zhang, Y. X., and Xu, Z. J. (1995) "Atomic Radii of Noble-Gas Elements in Condensed Phases". *Am. Mineral.* **80**, 670-675.

Zoski, C. (2007) "*Handbook of electrochemistry"*, Elsevier Science, Amsterdam.